This is to certify that the
thesis entitled

DESIGN CONSIDERATIONS FOR MICRO WAVE DISC ENGINES

presented by

MARCO VAGANI

has been accepted towards fulfillment
of the requirements for the

M.S. degree in Mechanical Engineering

Major Professor's Signature

12/10/08

Date

DESIGN CONSIDERATIONS FOR MICRO WAVE DISC ENGINES

By

Marco Vagani

A THESIS

Submitted to
Michigan State University
in partial fulfillment of the requirements
for the degree of

MASTER OF SCIENCE

Mechanical Engineering

2008

ABSTRACT

DESIGN CONSIDERATIONS FOR MICRO WAVE DISC ENGINES

By

Marco Vagani

With the increasing trend towards technological miniaturization, the demand for micro-scale power generation has been growing steadily. However, the downscaling of internal combustion and gas turbine engines has been hindered by losses in cycle efficiency at smaller scales. This thesis presents two concept micro wave disc engines which are specifically designed for micro-scale power generation.

A wave disc is an unsteady pressure exchange device that has a proven potential for gas turbine enhancement. It employs shockwaves within rotating micro-channels to directly transfer energy between two fluids. The first concept engine presented is the External Combustion Wave Disc Engine, which employs a wave disc to replace the low efficiency turbomachinery components in a micro gas turbine engine. The second concept engine is the Internal Combustion Wave Disc Engine, with combustion occurring within the micro-channels of the rotor.

The first part of this work discusses the operation principles for both wave disc engine concepts and the wave patterns developed for them using gas dynamics relations. The second part describes the numerical simulation of wave discs and the design methodology employed. For this purpose, an automated tool was developed to model and simulate wave disc operation using FLUENT. Finally, an approach for modeling and simulating the internal combustion wave disc engine is proposed.

To my wife and my parents

ACKNOWLEDGMENTS

I would like to start by expressing my gratitude toward Dr. Norbert Müller, whose vision and support have brought me to this point. I thank him for his faith in my talents, for his always helpful guidance, and for the freedom with which he allowed me to explore my work. I wish him all the best in his professional and personal life.

I would also like to thank Dr. Abraham Engeda and Dr. Criag Somerton, for agreeing to participate in my thesis committee and for their comments that helped me improve this work. I am especially grateful to Dr. Engeda for his support over the years and for all the opportunities he has allowed me to have in this field.

I would like to acknowledge the importance of Florin Iancu's work in this field. This thesis is a continuation on the work he started in this lab. In addition, I would like to thank all my colleagues and friends who helped make these years memorable. Luděk Pohořelský has made major contributions to this project; and with his help, knowledge, and motivation has improved the lab tenfold. I thank Pradeep Kumar, Kanishka Sharma and Pranav Sané, whose work has helped improve my own. I also thank Stephanie Bonner, who was always willing to put up with more work. Finally, I thank John Quackenbush, Jijo Joseph and Anirban Lahiri for their good spirits and perennial availability during the long hours in the lab.

Inoltre, vorrei ringraziare la mia famiglia, che mi hanno dato una tremenda opportunità nel mandarmi a studiare negli Stati Uniti. Finally, a special thanks to my wife for her help and understanding.

TABLE OF CONTENTS

LIST OF TABLES ..... **VI**

LIST OF FIGURES ..... **VIII**

NOMENCLATURE ..... **XI**

CHAPTER 1: INTRODUCTION **1**

CHAPTER 2: BACKGROUND **3**
2.1 MICRO-SCALE POWER GENERATION 3
2.2 PRESSURE EXCHANGE WAVE ROTOR TECHNOLOGY 9

CHAPTER 3: WAVE DISC ENGINE CONCEPTS **18**
3.1 EXTERNAL COMBUSTION WAVE DISC ENGINE 18
3.2 INTERNAL COMBUSTION WAVE DISC ENGINE 21

CHAPTER 4: WAVE PATTERNS AND 1-D DESIGN CODE **25**
4.1 SIMPLE WAVE PATTERN 25
4.2 IMPROVED WAVE PATTERN 30
4.3 1-D DESIGN CODE FOR WAVE DISC 34
4.4 WAVE PATTERN FOR INTERNAL COMBUSTION WAVE DISC ENGINE 36

CHAPTER 5: AUTOMATED WAVE DISC SIMULATION CODE **43**
5.1 NUMERICAL SIMULATIONS OF WAVE DISCS 43
5.2 GEOMETRY 45
5.3 MESH 50
5.4 PRE-PROCESSING SETUP 55
5.5 SIMULATION 59
5.6 POST-PROCESSING 62

CHAPTER 6: DESIGN METHODOLOGY AND RESULTS **65**
6.1 DESIGN METHODOLOGY 65
6.2 NUMERICAL COMPARISON AND VALIDATION OF WAVE PATTERNS 67
6.3 ENERGY CONSIDERATIONS 78

CHAPTER 7: SUGGESTIONS FOR FUTURE WORK **87**
7.1 OPTIMIZATION FOR NUMERICAL SIMULATION CODE 87
7.2 CFD SIMULATIONS OF INTERNAL COMBUSTION WAVE DISC ENGINE 88

CHAPTER 8: CONCLUSIONS **93**

APPENDIX **95**

REFERENCES **100**

LIST OF TABLES

Table 1. Sample operating points for 1-D design code, results shown in Figure 19 35

Table 2. Sample operating point for internal combustion wave disc engine, result shown in Figure 22 42

Table 3. Input variables necessary for generation of porting geometry 47

Table 4. Input variables necessary for generation of straight and curved channels 49

Table 5. Input variables necessary for FLUENT pre-processing setup and simulation ... 59

Table 6. General geometry and operation parameters for numerical comparison of wave patterns 67

Table 7. Porting angles calculated using simple wave pattern 68

Table 8. Porting angles calculated using 1-D design code and improved wave pattern ... 72

Table 9. Porting angles determined for final wave pattern iteration 75

Table 10. Comparison of velocity magnitudes at the inlets and outlets of the inviscid and laminar models 76

Table 11. Values and resulting specific work for final porting design with straight channels and ports 79

Table 12. Inlet and outlet port angles for a straight channel rotor, shown in Figure 40 ... 80

Table 13. Values and resulting specific work for wave disc with straight channels and angled ports 82

Table 14. Values and resulting specific work for wave disc with curved channels 85

Table 15. Geometric and operating conditions for wave disc simulation of simple wave pattern. Results shown in Figure 36. 95

Table 16. Geometric and operating conditions for wave disc simulation of improved wave pattern. Results shown in Figure 37. 96

Table 17. Geometric and operating conditions for wave disc simulation of final iteration of wave pattern. Results shown in Figure 38 and Figure 39. 97

Table 18. Geometric and operating conditions for wave disc simulation with angled porting. Results shown in Figure 40. 98

Table 19. Geometric and operating conditions for wave disc simulation with curved channels. Results shown in Figure 41. 99

LIST OF FIGURES

Images in this thesis are presented in color

Figure 1. Specific energy for hydrocarbons and several battery technologies [10] 4

Figure 2. MIT micro gas turbine engine generator [8] 7

Figure 3. Micro-turbine (left) and micro-compressor (right), produced by MIT, etched out of a silicon wafer, with diameters of 4 mm and 8 mm [7] 8

Figure 4. Cutaway of the micro gas turbine engine assembly [7] 8

Figure 5. Schematic model of a through-flow wave rotor and porting 10

Figure 6. NASA four port wave rotor drum (left) and Comprex® rotor drum (right) 11

Figure 7. Schematic for a wave rotor enhanced gas turbine engine in a) through-flow and b) reverse-flow configurations 12

Figure 8. Temperature-Entropy diagram for a gas turbine engine with and without wave rotor topping 13

Figure 9. Schematic for a wave rotor enhanced micro gas turbine engine design 14

Figure 10. Micro-scale wave disc, the bottom showing a cutaway view of the rotor channels 16

Figure 11. Schematic for a radial wave disc enhanced micro gas turbine engine design. 16

Figure 12. Temperature-Entropy diagram for an external combustion wave disc engine 19

Figure 13. External combustion wave disc engine configuration 20

Figure 14. Wave disc engine with a reverse-flow, two combustion chamber configuration 21

Figure 15. Temperature-Entropy diagram for internal and external combustion wave disc engines 22

Figure 16. Schematic for the internal combustion wave disc engine 23

Figure 17. Simple wave pattern for a through-flow wave rotor 26

Figure 18. Improved wave pattern for a through-flow wave rotor 31

Figure 19. Wave pattern outputs for two operating points.
Left – Fully scavenged rotor. Right – EGR Present. 36

Figure 20. Wave diagram for a wave disc with internal combustion 37

Figure 21. Wave diagram for an internal combustion wave disc shown in absolute reference frame 39

Figure 22. Wave pattern output for an internal combustion wave disc engine 42

Figure 23. Schematic of the input variables necessary for the porting geometry 46

Figure 24. Schematic of the input variables necessary for a straight channel 48

Figure 25. Schematic of the input variables necessary for a curved channel 49

Figure 26. Close-up of inner gap for a structured grid, aligned with geometric features. 50

Figure 27. Close up of inner gap for a semi-structured grid, with skewed mesh within gap 51

Figure 28. Close-up of high pressure zone with a coarse mesh,
with 270 radial mesh points and 50 tangential mesh points 52

Figure 29. Close-up of high pressure zone with a fine mesh,
with 540 radial mesh points and 100 tangential mesh points 53

Figure 30. Complete mesph for a 4-cycle wave disc with curved channels and angled porting 54

Figure 31. Full model of the 4-cycle wave disc with curved channels and angled porting 55

Figure 32. Numerical error present in coupled solver during transient start-up 57

Figure 33. Wave disc pressure contours during initialization, transient start-up, and steady-state operation 61

Figure 34. Graphical user interface for FLUENT post-processing interface 63

Figure 35. Flowchart of design methodology 66

Figure 36. Pressure and temperature contours for a wave disc using the simple wave pattern 69

Figure 37. Pressure and temperature contours for a wave disc using the improved wave pattern 71

Figure 38. Pressure and temperature contours for a wave disc using final wave pattern iteration 74

Figure 39. Pressure and temperature contours for final wave pattern iteration using a laminar solver 77

Figure 40. Pressure and temperature contours for a wave disc with angled porting 81

Figure 41. Pressure and temperature contours for a wave disc with curved channels..... 84

Figure 42. Possible geometry and mesh for the channels of an internal wave disc engine 90

Figure 43. Heat addition zone for internal combustion wave disc modeling 91

NOMENCLATURE

a	Speed of sound	[m/s]
c	Number of cycles per revolution	dimensionless
$c_{\theta 1}$	Inlet absolute tangential velocity	[m/s]
$c_{\theta 2}$	Outlet absolute tangential velocity	[m/s]
gap	Gap size	[m]
H	Enthalpy	[kJ]
h	Specific enthalpy	[kJ/kg]
L	Length of channel	[m]
L_{inner}	Length of inner porting	[m]
L_{outer}	Length of outer porting	[m]
$\dot{m}$	Mass flow rate	[kg/s]
N	Rotational velocity of rotor	[rpm]
N_{cycles}	Number of full cycles to be simulated	dimensionless
$N_{solution}$	Number of iterations for a full solution	dimensionless
P	Pressure	[Pa]
Q	Heat transfer	[kJ]
R	Gas constant	[kJ/kg·K]
r	Radius	[m]
T	Temperature	[K]
$T_{turbine}$	Turbine inlet temperature	[K]
u	Flow velocity	[m/s]
U	Internal energy	[kJ]

U_1	Inlet blade velocity	[m/s]
U_2	Outlet blade velocity	[m/s]
u_{head}	Expansion wave head velocity	[m/s]
u_p	Induced flow velocity	[m/s]
u_{tail}	Expansion wave tail velocity	[m/s]
V	Volume	[m^3]
w	Shockwave velocity	[m/s]
W	Work	[kJ]
W_{comp}	Compression Work	[kJ]
$\dot{W}$	Rate of work	[kJ/s]
γ	Specific heat ratio	dimensionless
ΔR	Channel length	[m]
Δt	Simulation time step size	[s]
$\Delta t_{iterations}$	Maximum iterations per time step	dimensionless
ΔW	Specific work	[kJ/kg]
$\Delta \Phi$	Channel unit size	[deg]
θ	Angle	[deg]
Π_S	Pressure ratio across shockwave	dimensionless
τ	Torque	[N·m]
φ	Channel thickness	[deg]
ω	Rotational velocity of rotor	[rad/s]

Subscripts

1	Air inlet conditions / Conditions in front of wave
2	Air outlet conditions / Conditions behind wave

3	Exhaust inlet conditions
4	Exhaust outlet conditions
close	Port closing
f	Final conditions
i	Initial conditions
inner	Inner radius
open	Port opening
outer	Outer radius
p	Product conditions
r	Reactant conditions
ref	Reference conditions

Acronyms

AI	Air inlet
AO	Air outlet
CC	Combustion Chamber
CFD	Computational Fluid Dynamics
E	Expansion Wave
EC	External Combustion
EGR	Exhaust Gas Recirculation
EI	Exhaust inlet
EO	Exhaust outlet
IC	Internal Combustion
MAV	Micro Air Vehicles
MEMS	Micro Electrical Mechanical Systems

P	Pressure Wave
S	Shockwave
UAV	Unmanned Air Vehicles
WD	Wave Disc
WDE	Wave Disc Engine
WR	Wave Rotor

CHAPTER 1: INTRODUCTION

The development of micro power generation engines employing Micro Electrical Mechanical Systems technology has been strongly intensified in recent years. However, the creation of such devices has been largely hindered by losses in cycle efficiency at smaller scales. The scaling of conventional engines such as internal combustion and gas turbine engines faces major difficulties with heat loss, component efficiencies, friction, sealing, fabrication and assembly.

This work proposes two concept engines, micro wave disc engines. They are a novel idea for micro-scale power generation. In such devices, external or internal combustion is used to generate shockwaves that can enhance combustion and allow for compression and expansion of the operating gases.

Chapter 2 is a review of the benefits of micro-scale power generation and its applications, focusing also on the MIT micro gas turbine project. It also contains a review of wave rotor technology and the development of the wave disc for micro gas turbine enhancement.

Chapter 3 presents the concept of a Wave Disc Engine, which uses wave disc technology to replace the steady-state turbomachinery components in micro gas turbines. Two separate concepts are developed, with external combustion and internal combustion. The External Combustion Wave Disc Engine uses a pressure-exchange wave disc to compress and expand the working fluids. The Internal Combustion Wave Disc Engine is a novel concept that includes combustion within the channels of the wave disc.

Chapter 4 explains the wave patterns developed for wave disc technologies. Two different patterns are presented for wave discs as pressure exchangers. The first pattern is greatly simplified to reduce calculation time. The second pattern is much more accurate than the first, introducing various gas dynamics principles that were not taken into account in the simplified version. In order to solve the improved wave pattern, a 1-D design code was developed. This chapter also explains the wave pattern and similar code developed for an internal combustion wave disc.

Chapter 5 introduces the need for numerical simulations in order to validate and improve on the results of the 1-D design code. An automated simulation tool was developed to perform these numerical analyses using FLUENT, a common computational fluid dynamics software. The tool's geometric and meshing parameters are explained, along with the solver setup and simulation process.

Chapter 6 first introduces the new design methodology for wave discs that was developed. This methodology would not be possible without the 1-D design tools described in Chapter 4 and the 2-D numerical simulation tool described in Chapter 5. This chapter then proceeds to apply this design methodology on a wave disc design. Both of the wave patterns developed in Chapter 4 are simulated, and their results are combined to produce a final, more effective wave disc design.

Chapter 7 outlines directions for future work. This includes the possibility of using optimization software to improve the results of the numerical simulation code. It also provides a possible approach to modeling and simulating the Internal Combustion Wave Disc Engine. Finally, Chapter 8 summarizes the conclusions drawn form this work.

CHAPTER 2: BACKGROUND

2.1 MICRO-SCALE POWER GENERATION

Modern technological society has an increasing need for smaller power generation devices. With the developing trend towards the miniaturization of electronic and mechanical devices, the demand for high efficiency power generation units is growing steadily. This demand is largely focused on finding a viable alternative to chemical batteries.

The demand for smaller, lighter, highly efficient systems and devices requires the integration of both electrical and mechanical systems in progressively smaller devices. This field, called Micro Electrical Mechanical Systems (MEMS), appeared towards the end of the 20^{th} century through the creation of integrated sensors and actuators. MEMS combines electrical and mechanical engineering concepts with micro-fabrication technology to create fully integrated systems on silicon chips. Currently, the field has expanded to a variety of applications, from audio-visual implants to complete fluid micro-systems, including power generation.

The development of MEMS has spurred research in the energy field, directed towards reducing the scale of common power sources. This led to the design of micro-heat engines such as internal combustion engines, gas turbines, and steam turbines. This field is called MEMS Power Systems, or Power MEMS [8]. The objective of this field is to create smaller, sub-centimeter scaled engines that produce 10 to 100 watts with power densities and performances comparable to their larger-scale counterparts.

Power MEMS engines provide a huge advantage over common chemical batteries. The liquid fuels used in such engines have a much larger energy density than most batteries, as shown in Figure 1. Even only at 5% efficiency, a small octane engine would have a comparable energy density to that of a battery [10]. This means that devices powered by a micro-scale engine can be lighter and smaller than an equivalent battery powered device. They could operate for a longer period of time and may even be refueled. This even reduces the manufacturing and waste disposal costs associated with chemical batteries.

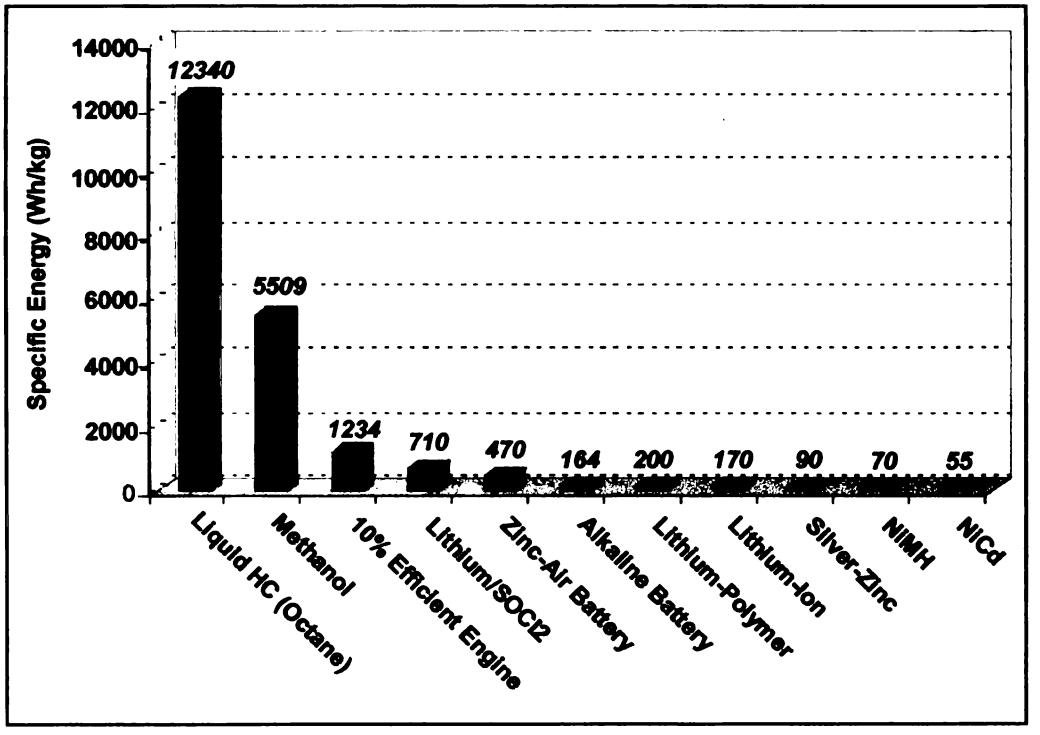

Figure 1. Specific energy for hydrocarbons and several battery technologies [10]

The most anticipated application for Power MEMS engines is the creation of portable power generation. With small, efficient power sources, it would be possible to replace or enhance batteries in most common applications. This includes laptop computers, cell phones, and other common electronic devices. Micro-engines built into these devices could provide a constant source of power that could outlast the common

batteries used. Alternatively, they could be used to recharge the battery when its charge is too low, running only for short periods of time. [25,38]

The largest field of applications for Power MEMS engines is in the defense industry. Unmanned air vehicles (UAV) and micro air vehicles (MAV) are being developed of increasingly smaller sizes [13,30]. Three important factors in the development of these vehicles are the size, weight and range of the design. Micro-scale engines would be able to improve on these three issues while still providing the power necessary [37]. The small size and lightweight materials used in micro-heat engines provide a big improvement over traditional power sources, and their high efficiency and energy density will allow the vehicle to have a much larger range than one powered by battery cells. An additional electric flight concept includes micro-engines within the aircraft wings creating both electrical power and additional lift [22].

Furthermore, the increasingly high-tech devices used by soldiers and reconnaissance vehicles require them to carry bulky, heavy battery packs around for portable power [14,12]. The light weight of a micro-engine would provide a vast improvement for soldier packs, making them smaller and lighter. Also, the higher energy density of liquid fuels would allow them to carry smaller fuel reservoirs rather than large batteries.

Currently most MEMS devices draw power from macroscopic power supplies such as external batteries. This limits their functionality in many applications [20]. Integrating MEMS micro sensors and actuators with micro-heat engines will improve the scope and application range of such devices. Bulky and inefficient energy storage devices may be eliminated. Additionally, a power-independent MEMS device does not require

electrical connections to external power sources, giving it improved mobility and autonomy.

Another benefit of micro-scale power includes the possibility of having multiple backup power sources when the main source fails. This would be ideal for applications where certain components must retain functionality after a power shortage. Multiple small or micro-scale engines could power these components, making them independent of the main power generator or grid.

The promise for flexible, energy-independent, multiple-application devices has led micro-scale power generation to become a forefront research topic in the energy industry. There have been significant recent attempts to miniaturize conventional combustion engines for small-scale application, using MEMS or other fabrication methods, to create micro-scale power generation devices. Well publicized among these are the MIT micro gas turbine engine [7,8], the UC Berkeley mini rotary engine [11,31], and the Georgia Tech and Honeywell-U. Minnesota free-piston engines [1].

The MIT Micro Gas Turbine Engine Project was begun in 1995 with the objective of using it for power generation and small aerial vehicle propulsion. A cross-section schematic of the engine is shown in Figure 2. The basic design is composed of a supersonic, radial compressor and turbine, with an annular ring combustion chamber. The compressor includes diffuser vanes, and the turbine includes swirl vanes. They are connected by a hollow shaft. The high rotational speeds of the rotor required gas film bearings in order to reduce friction. The previously existing MEMS dry-friction bearings would not have an acceptable operating life at the required speeds [5]. The final design included a journal and thrust gas film bearings. Hydrogen gas is the fuel used, injected

directly after the compressor vanes. A motor-generator is built within the engine in order to start the rotor and produce electrical power. The built-in motor provides the advantage of reducing the number of parts and bearings necessary. The engine is designed to produce 20 kW of electrical power when using pre-compressed inlet air [8].

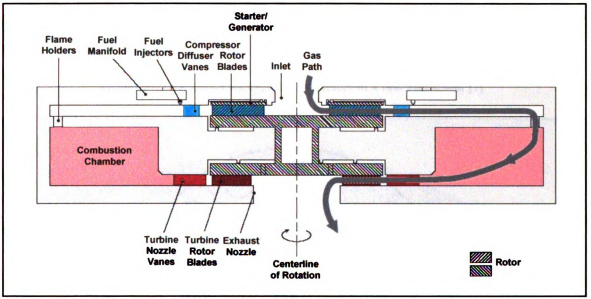

Figure 2. MIT micro gas turbine engine generator [8]

Initially, the material chosen for micro-fabrication was silicon, but later research proved that a layer of silicon carbide would strengthen the material and allow it to withstand higher temperatures. The turbine and compressor were designed radially to ease the micro-fabrication process, which prefers structures with an extruded 2-D cross-section. Two examples of micro-fabricated rotors produced by MIT on a silicon wafer are shown in Figure 3. The entire engine assembly consists of nine micro-fabricated wafers (layers), bonded together. A cutaway of the bonded assembly is shown in Figure 4.

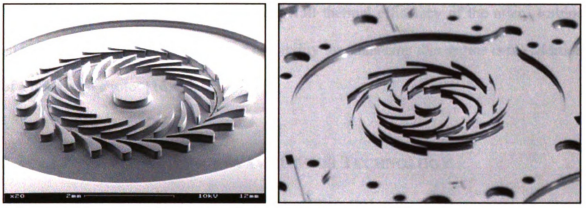

Figure 3. Micro-turbine (left) and micro-compressor (right), produced by MIT, etched out of a silicon wafer, with diameters of 4 mm and 8 mm [7]

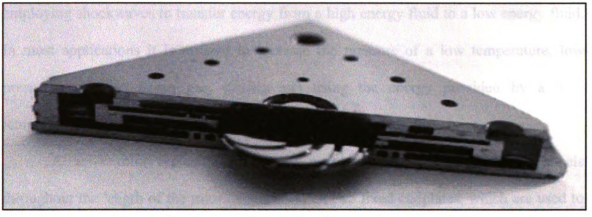

Figure 4. Cutaway of the micro gas turbine engine assembly [7]

The MIT engine attempts to scale the compressor, combustor, and turbine of a conventional gas turbine engine using micro-fabrication methods. The functional principle and thermodynamic cycle are the same as conventional gas turbines. Turbo-component performance, however, suffers due to the downsizing effect. It was shown that the polytropic efficiency of conventional steady-state turbomachinery decreases with size [7]. The increased influence of wall effects decreases the turbo-component's efficiency, since flow velocities remain similar while the channel dimensions are reduced. The continuous flow combustor suffers from increased heat loss at micro-scale, where the rate of heat loss is larger than the rate of heat production through combustion.

With lower component efficiencies, the overall thermal efficiency of the micro turbine engine is significantly decreased. One possibility for enhancing this engine is the addition of a micro wave rotor [16,17].

2.2 PRESSURE EXCHANGE WAVE ROTOR TECHNOLOGY

A wave rotor is an unsteady flow device that utilizes the concept of direct pressure transfer between fluids through waves. It is used as a pressure exchanger, employing shockwaves to transfer energy from a high energy fluid to a low energy fluid. In most applications it is utilized to increase the pressure of a low temperature, low pressure gas (the driven gas, usually air) using the energy provided by a high temperature, high pressure gas (the driver gas, usually exhaust gas).

A wave rotor typically consists of a rotating drum with straight channels throughout the length of the rotor. It lies between two fixed endplates, which are used to seal the channels from the manifold. The fixed plates contain ports, which allow the channels to be periodically exposed to the driver and driven gases. The sudden exposure to these gases initiates shockwaves or expansion waves within the channels. A schematic of a wave rotor is presented in Figure 5. The channels are exposed to a high pressure, high temperature gas at the Exhaust Inlet port (EI) and to low pressure, low temperature air at the Air Inlet (AI) port at the inlet side of the rotor. After the energy exchange within the rotor is complete, the outlet side of the channels is opened to release the pressurized, low temperature air at the Air Outlet (AO) port, and the expanded, high temperature gas, at the Exhaust Outlet (EO) port.

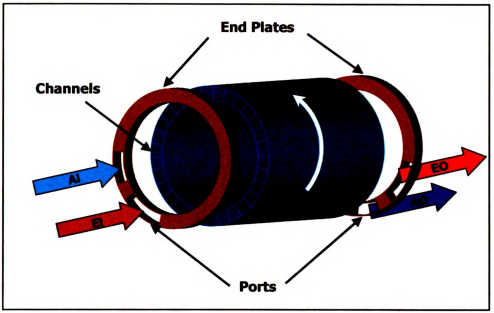

Figure 5. Schematic model of a through-flow wave rotor and porting

The operating principle of the wave rotor allows it to compress the inlet air while expanding the exhaust gas. In this manner, the wave rotor acts as both an air compressor and a gas turbine, but within a single rotating part. This is achieved using lower flow velocities and a smaller rotational speed than traditional turbomachines. The periodic exposure to hot gas and cool air allows the rotor to maintain lower operating temperatures, having a "self-cooling" effect.

Multiple applications have been found for wave rotor technology. Figure 6 shows two wave rotors, the first of which was produced and tested by NASA as a performance enhancer to a gas turbine engine [35]. The second wave rotor depicted was produced by Brown Boveri Corporation. This wave rotor, named the Comprex®, has been used commercially in the Mazda 626 Capella as a supercharger for the internal combustion engine, which sold more that 150,000 units [21].

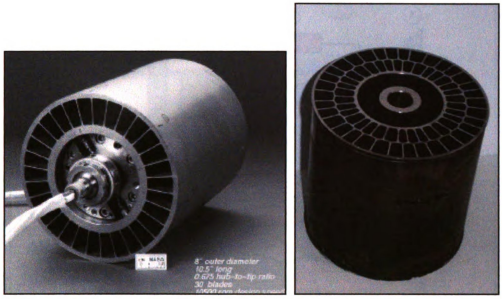

Figure 6. NASA four port wave rotor drum (left) and Comprex® rotor drum (right)

A wave rotor may be used to enhance the performance of a gas turbine engine. The rotor would operate in parallel to the combustion chamber, using the pre-compressed air from the traditional compressor as its inlet air, its driven gas. This air would be compressed further and sent to the combustion chamber. The combustion chamber exhaust would be the driver gas, and the rotor would then supply pre-expanded exhaust to the turbine.

The wave rotor may be driven by an external motor or may be designed to be self-driven, using the momentum of the flow to rotate the rotor. The operation principle is analogous to the operation of a supercharger or turbocharger in an automotive engine. The wave rotor increases the pressure of air entering the combustion chamber and expands the exhaust gas leaving it. This has the effect of increasing the total work output of the engine.

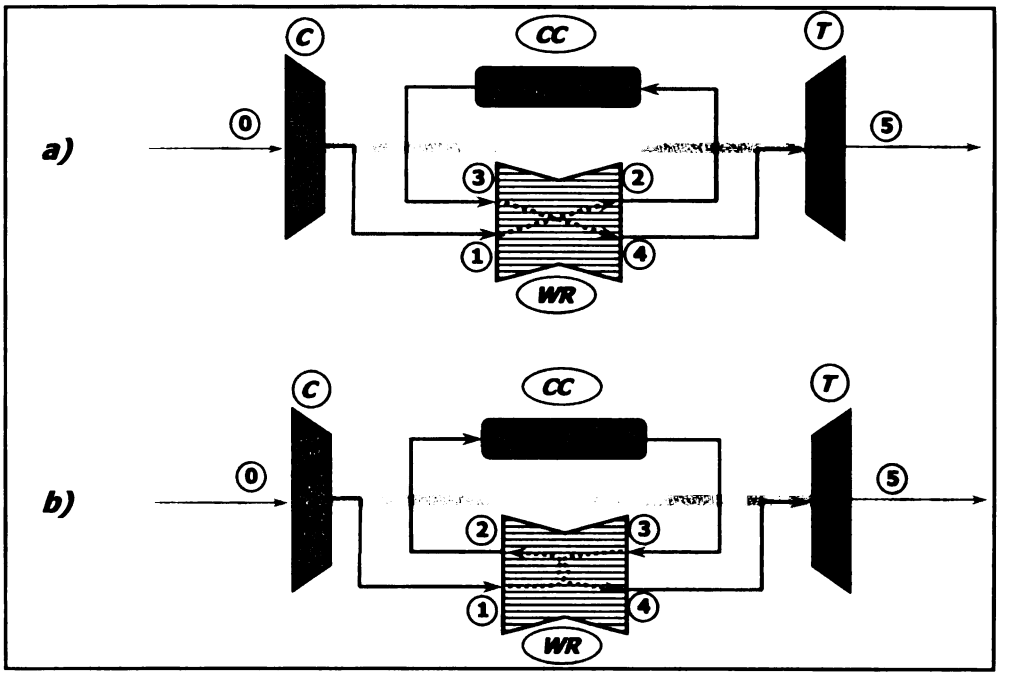

Figure 7. Schematic for a wave rotor enhanced gas turbine engine in a) through-flow and b) reverse-flow configurations

Figure 7 depicts the cycle schematics for two possible configurations of the wave rotor for gas turbine engine topping. In the through-flow configuration, the two flows travel the length of the rotor in the same direction, so that the rotor has an inlet side and an outlet side. In the reverse flow configuration, the two flows exit from the same side that they enter. This results in a hot side and a cold side.

In both configurations shown above, the inlet air (0) is initially compressed by the compressor. It then reaches the air inlet (AI/1) port on the wave rotor, where it is ingested into the rotor channels. Once it comes in contact with the hot exhaust gas (EI/3), a shockwave is created which further compresses the fresh air. This air is then evacuated from the channel and is sent to the combustion chamber (AO/2). Finally, the exhaust gas is evacuated by means of the expansion waves created by the sudden closing of the channel's inlet ports (EO/4). This exhaust gas, which loses some pressure in the process, is then supplied to the turbine for work extraction (5).

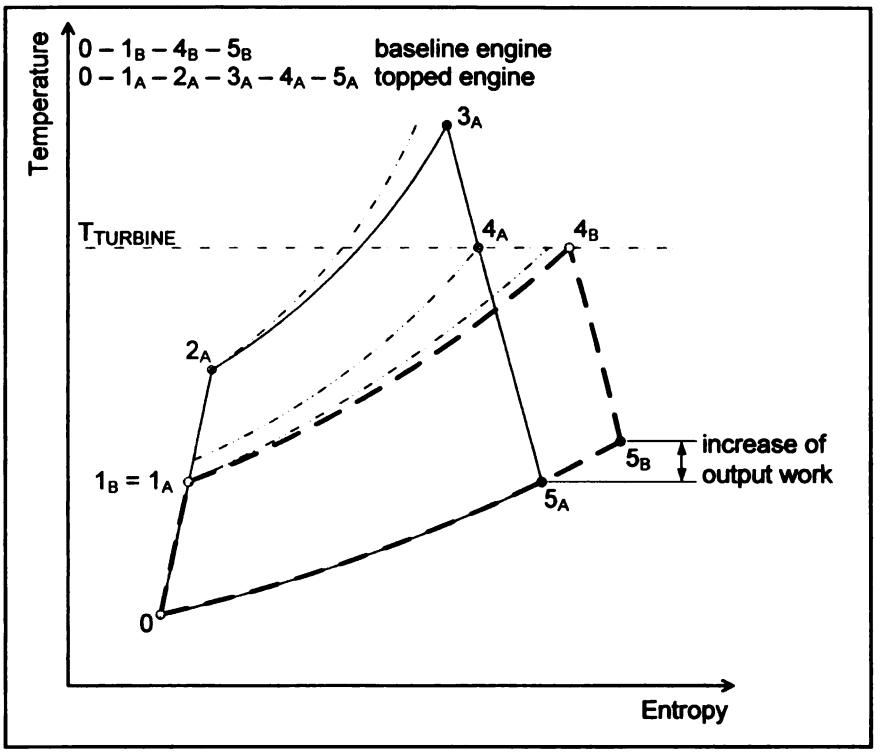

Figure 8. Temperature-Entropy diagram for a gas turbine engine with and without wave rotor topping

The advantage provided by the wave rotor is apparent when comparing a wave rotor enhanced cycle with a baseline cycle. The two cycles, shown in Figure 8, are compared for equivalent compressor pressure ratios and turbine inlet temperatures. The amount of heat addition in the combustor is the same for both cycles, and the combustion pressure loss is shown for both.

The pressure increase provided by the wave rotor allows combustion to occur at a higher pressure than for the baseline engine. After the pre-expansion of the exhaust gas in the wave rotor, the exhaust enters the turbine at a higher pressure than for the baseline cycle. In fact, the pressure increase provided by the wave rotor allows the turbine inlet pressure to be higher than the pressure at the outlet of the compressor. The larger pressure ratio across the turbine results in added work extracted from the flow. The work output increases while the input work to the compressor remains the same. This improves the

cycle's thermal efficiency. The wave rotor topped gas turbine engine extracts more work and is more efficient than the baseline engine.

The potential improvement of the gas turbine engine cycle provided by the implementation of a wave rotor makes it an ideal candidate for micro-scale power generation. For micro-scale applications, it is necessary to achieve high thermal efficiency. With a higher efficiency, the wave rotor topped engine can output more power while taking up the same space and weight. The following two designs were proposed to enhance a micro gas turbine engine similar to the MIT Micro Gas Turbine Engine [17].

The first design uses a conventional wave rotor configuration, as a rotating drum with channels running along its length, as shown in Figure 9. The wave rotor drum is attached to the outer radius of the rotating compressor/turbine assembly. The combustion chamber continues to be an annulus, on the outside edge of the micro-engine. Being a through-flow design, the fresh air from the compressor enters the wave rotor channels and travels through the rotor to the turbine side of the engine. The compressed air is then ducted into the combustion chamber, mixed with fuel and ignited. The combustion gas re-enters the rotor, is expanded, and exhausts to the turbine.

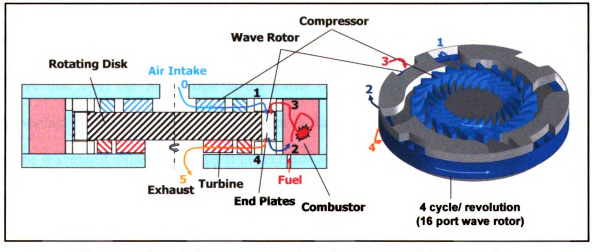

Figure 9. Schematic for a wave rotor enhanced micro gas turbine engine design

In this configuration, the wave rotor produces the desired pressure boost for the engine, but also has a few more advantages. With the wave rotor attached to the end of the rotating turbine/compressor disc, there is no need for a separate drive for the wave rotor itself. Additionally, the self-cooling characteristic of the wave rotor helps isolate the rotating parts in the center of the engine from the heat produced by the combustion chamber.

However, the drawbacks of this design include the fact that it requires a small increase in diameter in order to accommodate for the wave rotor. Furthermore, the wave rotor configuration is not ideal for micro-fabrication. Its surface to height ratio is very small, having a very narrow 2-D surface that is extruded for a long length. This requires much more complicated micro-fabrication methods in order to ensure accurate sizes and straight channels.

The difficulty in creating a wave rotor using micro-fabrication processes led to the creation of the radial-flow wave rotor, otherwise called a wave disc [27]. The wave disc has channels that are located radially along a rotating disc. In this configuration, the porting is placed on the inner and outer radii of the rotor. The large surface area and short height of the rotor made it ideal for the micro-fabrication process. Two halves of the rotor would be fabricated from two wafers and bonded together. One more added benefit of the wave disc over the wave rotor is the radial configuration allows the design to take advantage of the centrifugal forces present in the channels. These forces allow the rotor to be scavenged more thoroughly if the exhaust outlet port is placed on the outer radius of the rotor. One possible configuration for a micro wave disc is shown in Figure 10.

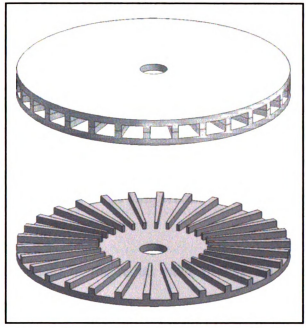

Figure 10. Micro-scale wave disc, the bottom showing a cutaway view of the rotor channels

The second topped micro gas turbine engine design includes the implementation of the wave disc, as is shown in Figure 11. It is located above the combustion chamber, on the compressor side of the engine. The inlet air is fed directly from the compressor, and travels through the disc to the combustion chamber. After combustion, the exhaust gas is again expanded through the rotor and ported to the turbine.

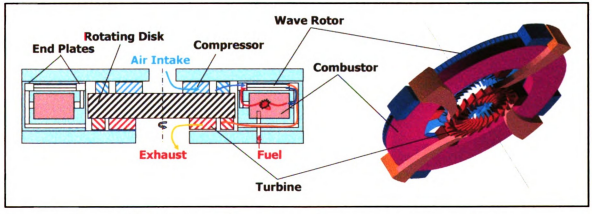

Figure 11. Schematic for a radial wave disc enhanced micro gas turbine engine design

In this configuration, the wave disc provides a few advantages over the wave rotor. While still producing the same pressure boost, the disc is much simpler to

manufacture in micro-scale. The radial shape of the wave disc allows the micro-engine to occupy the same diameter as the baseline engine. The disc does not have to be attached to the main shaft, and can be self-driven by using the momentum of the flow through it. The improved scavenging provided by the centrifugal forces in the disc allows it to attain a lower average temperature than the wave rotor, where exhaust gas recirculation has been shown to create concentrated, high-temperature areas that negatively affect its performance [23].

Another added benefit of the radial wave disc is the possibility of using it to extract energy from the flow. In gas turbine engine topping applications, it is sufficient for the wave disc to extract enough energy from the flow to become self-driven. However, by using angled porting, the rotor may be capable of extracting more energy than is needed to drive it. This energy could be harnessed to generate power. Modifying the channels so that they are curved, rather than the traditional straight channel design could improve the energy extraction of the wave disc even further.

CHAPTER 3: WAVE DISC ENGINE CONCEPTS

The possibility of extracting energy from the flow using only a wave disc has opened a promising new research area, Wave Disc Engines (WDE). The following sections present two different WDE concepts. The first replaces the turbine and compressor with a wave disc. The combustion chamber remains separate from the rotor; therefore it is designated as an External Combustion (EC) Wave Disc Engine. The second concept engine requires combustion to occur within the channels of the wave disc. This concept is named the Internal Combustion (IC) Wave Disc Engine.

3.1 EXTERNAL COMBUSTION WAVE DISC ENGINE

The wave disc enhanced gas turbine engines presented in the previous chapter effectively combine traditional, steady-state turbomachinery with unsteady, shockwave compression. This leads to a higher thermal efficiency compared to the baseline MIT gas turbine engine. However, the low efficiency of the compressor and turbine at the micro-scale is a limiting factor to the engine's overall efficiency.

The basic concept behind External Combustion Wave Disc Engines is to simply replace the turbomachinery components with a single pressure exchange wave disc [26]. The thermodynamic cycle remains the same as that of traditional gas turbine engines, as shown in Figure 12. The wave disc alone provides the compression and expansion needed for the cycle to be completed. It also is designed to produce torque on its own, so not even the turbine is required. The wave disc itself acts as a compression, decompression and torque generation unit, but all in a single rotating part.

The efficiency of shock wave compression is not as affected at micro-scale as that of traditional steady-state turbomachinery components [15]. Therefore, the wave disc has a higher efficiency for the compression process, reducing the work requirement. Another added benefit of the wave disc is its self-cooling feature. The channels are periodically cooled by the fresh inlet air, so the rotor remains at a lower temperature than a gas turbine engine with an equivalent compressor pressure ratio. The wave disc can therefore handle a much higher peak temperature from the combustion chamber. Both of these effects can be seen in the thermodynamic cycle shown below. The overall efficiency of the wave disc engine is higher than that of the gas turbine engine.

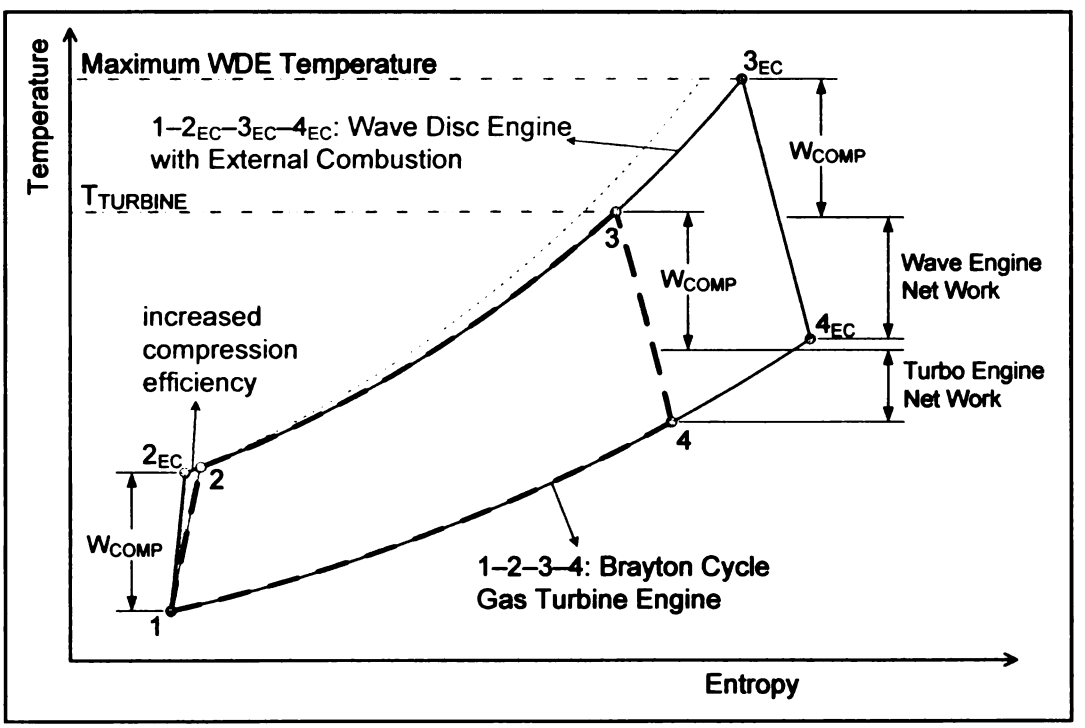

Figure 12. Temperature-Entropy diagram for an external combustion wave disc engine

The wave disc engine uses only one rotating part. Using an external drive would increase the overall size of the engine and introduce losses. Instead, a generator-starter is integrated within the engine itself, following the conceptual design developed by MIT [7,9]. This completely eliminates the mechanical losses associated with shaft

transmission. Additionally, the wave disc engine rotates at much lower speeds than a comparable compressor-turbine unit. This greatly reduces frictional losses and simplifies the bearing and the electric generator design.

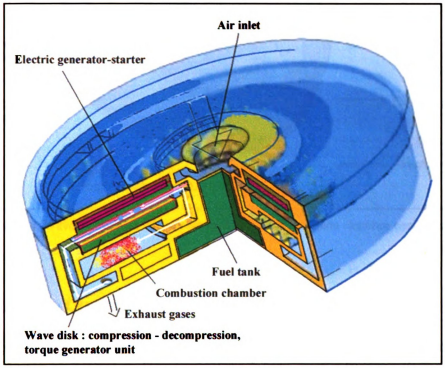

Figure 13. External combustion wave disc engine configuration

The EC wave disc engine shown in Figure 13 contains all of the features mentioned previously. Fresh air enters the center of the engine and is ported into the wave rotor channels. Shockwaves compress the air and send it to the combustion chamber, placed parallel to the disc. The hot exhaust gas is then redirected to the wave disc. After expansion, they are released through the bottom of the engine. Figure 14 is a better representation of the flow within the rotor. In the case depicted, the wave disc uses a reverse-flow configuration. This disc contains two cycles per revolution. The combustion chamber is split in half, using a separate combustion chamber for each cycle in the rotor.

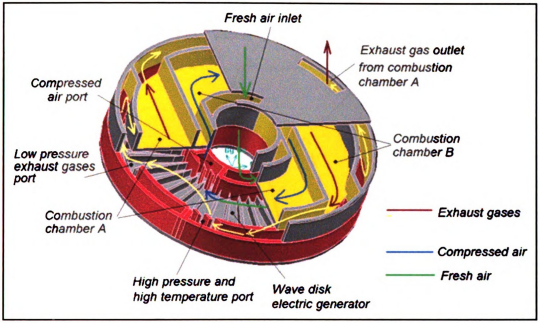

Figure 14. Wave disc engine with a reverse-flow, two combustion chamber configuration

3.2 INTERNAL COMBUSTION WAVE DISC ENGINE

The External Combustion Wave Disc Engine uses a typical open combustion chamber, where combustion occurs at a nearly constant pressure. However, the constant pressure combustion used for gas turbine engines and the wave disc engine is much less efficient than the confined combustion that occurs in Internal Combustion (IC) engines. This is a constant volume process, where both the temperature and pressure increase. The IC wave disc engine takes advantage of the confined combustion process by using the closed space within the rotor channels as a combustion chamber. During combustion, both ends of the channel are closed, so the process occurs at constant volume.

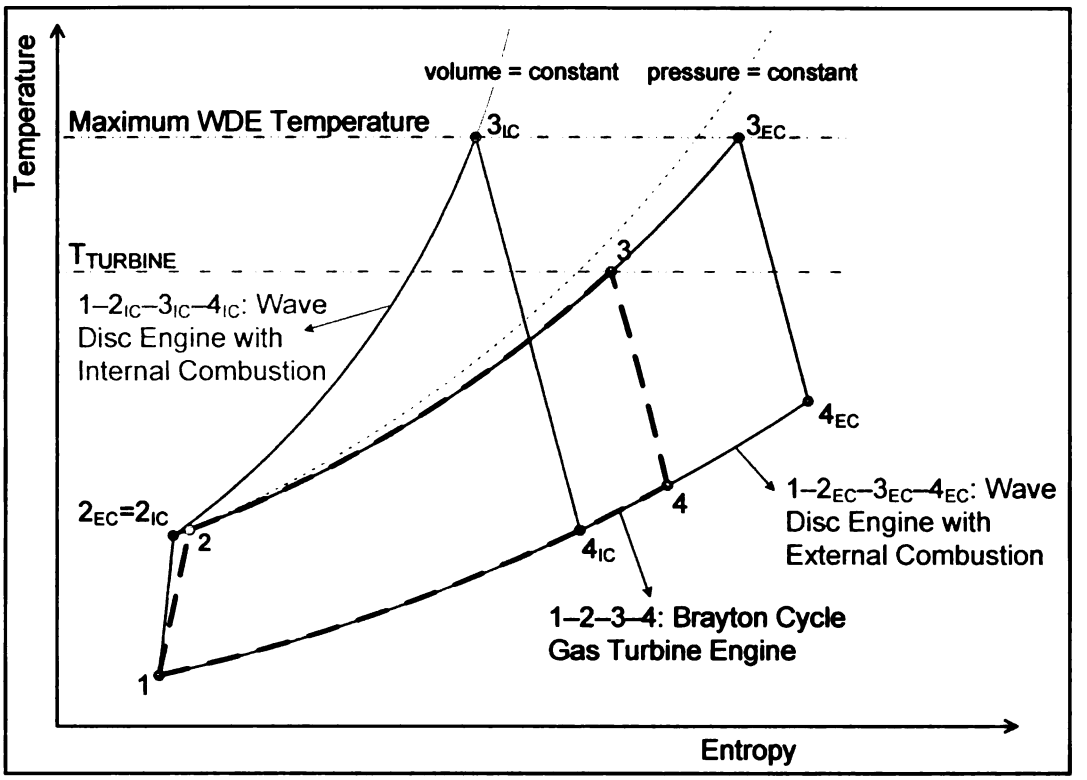

Figure 15. Temperature-Entropy diagram for internal and external combustion wave disc engines

Constant volume combustion provides a huge thermodynamic advantage. Figure 15 compares the cycles for the two types of wave disc engines. For the same peak temperature and compression ratio, the pressure after combustion is much higher for the IC wave disc engine. As a result, the pressure ratio during the expansion process is much larger, producing a significant increase in the extracted work by the engine.

The operation of the IC wave disc engine is very different from that of the EC wave disc engine. For this engine, only two ports are necessary. The inlet port intakes fresh air/fuel mixture, while the outlet port releases the burnt gas produced by the combustion. A schematic showing the operation principle of this engine is shown in Figure 16.

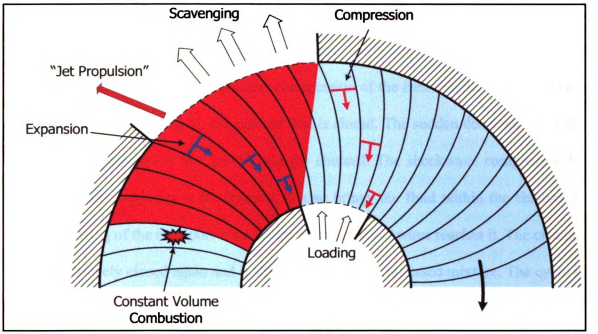

Figure 16. Schematic for the internal combustion wave disc engine

The channel begins with a fresh fuel/air mixture. It is closed on both ends, is rotating with the disc, and the fluid within it is at rest. The fuel/air mixture is then ignited, and the combustion process occurs at constant volume. This produces a large temperature and pressure rise within the channel.

After combustion is complete, the channel reaches the exhaust outlet port. The sudden opening of the boundary creates two effects. The high pressure within the channel, when suddenly released, has a "jet propulsion" effect which generates extra torque for the rotor. It also creates an expansion wave, which will travel the length of the channel and expand the exhaust gas within it. The expansion wave will force the exhaust gas out of the rotor.

When the expansion wave reaches the inlet side of the channel, the inlet port is opened. The flow created by the expansion wave will ingest fresh fuel/air mixture from that port. At this point, both ends of the channel are open, so the loading of fresh mixture

and scavenging of exhaust gas is taking place. Additionally, the centrifugal forces within the channel aid the scavenging and loading process.

The last step in the process is the compression of the fresh air/fuel mixture. Once the channel is fully scavenged, the exhaust port is closed. The sudden deceleration of the flow creates a shockwave that travels into the channel. The shockwave compresses the fuel/air mixture, preparing it for ignition. It also brings the fluid within the channel to rest. The closing of the inlet port is timed for when the shockwave reaches it. The channel is then completely closed again and is filled with fresh, compressed mixture. The cycle is complete and the channel is ready to be ignited to begin once again.

A few options are available for the compression process. The strength of the shockwave created by the sudden closing of the outlet port is dependant on the velocity of the flow through the channel at the moment it is closed. As explained above, it is possible to wait until the entire channel is scavenged before closing the exhaust outlet. However, if a stronger shockwave is required, it is possible to close the channel earlier in the cycle. This will create a stronger shockwave, but some exhaust gas will remain in the channel. This is called Exhaust Gas Recirculation (EGR). This may be beneficial to the combustion process, using the EGR gas to increase the temperature of the fuel/air mixture before ignition and limiting combustion to a smaller portion of the channel [34].

The Internal Combustion Wave Disc Engine takes advantage of the high efficiency of confined combustion, while having the high power density and low maintenance characteristics of continuous flow machines. It is physically simple and compact, using only one rotating part with a simple extruded 2D geometry. This will lead to a much lower unit cost compared to other competitive technologies.

CHAPTER 4: WAVE PATTERNS AND 1-D DESIGN CODE

4.1 SIMPLE WAVE PATTERN

The wave rotor and wave disc operate by transferring energy between two fluids using a set of shockwaves and expansion waves. These waves are created within the channels by the opening and closing of the inlet and outlet ports. These events are timed to ensure the correct wave pattern is formed within the rotor. The design of wave rotors and wave discs consists of determining the timing for each port based on their thermodynamic conditions. From the pressure and temperature conditions at each port, it is possible to develop a wave pattern for the flow within the channels. From this pattern, it is then possible to determine the timing of each port and design the porting for the device.

Multiple wave patterns have been developed for both trough-flow and reverse-flow wave rotors. The wave pattern presented in Figure 17 is based on the pattern developed by NASA for a four port, thorough-flow wave rotor [36]. The horizontal axis represents the position within the channel, and the vertical axis represents time. This pattern may be applied to both axial wave rotors and radial wave discs. Since the pattern depends only on the length of the channel and the timing of the ports, it provides a good initial design. However, the pattern does not take into account the added centrifugal forces that are present within the wave disc.

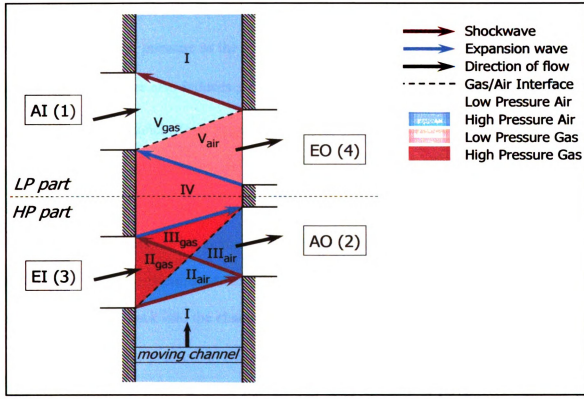

Figure 17. Simple wave pattern for a through-flow wave rotor

The porting for the through-flow wave pattern is clearly divided into an inlet side and an outlet side. In addition, the wave pattern is also divided into a high pressure (HP) part, and a low pressure (LP) part. The exhaust inlet port (EI) supplies high pressure, high temperature exhaust gas, while the air inlet port (AI) supplies low pressure, low temperature air. The air outlet port (AO) will be supplied with air at a higher pressure than the EI port, but only a slightly higher temperature than the AI port. The exhaust outlet port (EO) will be supplied with exhaust gas that is at a pressure between the AI and EI ports. The temperature at the EO port will be slightly lower than that of the EI port.

The pressure exchange process, as shown above, begins with a moving channel, filled with low pressure, low temperature air (Zone I). At this point, the through-flow velocity of the channel is zero. Once the EI port is opened, the pressure difference between the channel air and the port gas creates a shockwave (S_1), which propagates

towards the outlet side, into the channel. As S_1 moves into the channel, it compresses the air within it to same pressure as the EI port, with only a slight raise in temperature (Zone II_{air}). The shockwave also induces a flow behind it, causing hot exhaust gas from the EI port to enter the channel (Zone II_{gas}). The velocity induced by the shockwave is less than the velocity of the shockwave itself, producing a clear division between the gas and air in Zone II. This is called the gas/air interface.

The first shockwave reaches the end of the channel and reflects, creating a second shockwave (S_2). The opening of the AO port is timed to match this reflection. This new shockwave moves back into the channel and compresses both the air and gas in Zone II to a higher pressure, the pressure of the AO port, creating Zone III_{air} and Zone III_{gas}. The air and gas continue to move through the channel. The air, now at its desired pressure, is outlet through the AO port.

Once the second shockwave reaches the inlet side of the rotor, the EI port is closed. This prevents further gas from entering the channels. In addition, the sudden closing of the port creates an expansion wave (E_1) that moves into the channel. The expansion wave decreases the pressure of the gas, but also slows the flow down so its velocity is zero. The AO port is closed once the E_1 reaches the end of the channel. With this timing, the velocity in the entire channel is zero, and the exhaust gas is partially expanded (Zone IV).

The channel next reaches the low pressure part of the wave pattern. The flow is again initiated by the opening of the EO port. This sudden opening generates a new expansion wave (E_2), which reduces the pressure of the exhaust gas to its final state (Zone V_{gas}). E_2 also increases the velocity of the fluid, forcing it out of the EO port.

When the expansion wave reaches the inlet side of the channel, the AI port is also opened. Due to the induced velocity by the expansion wave, the air from the port moves into the channel (Zone V_{air}). The gas/air interface appears again, and moves towards the outlet side of the channel, scavenging the exhaust gas from the rotor.

Once the exhaust gas has been completely removed from the channel, the EO port closes. Due to this sudden closing, a weak shockwave (S_3) is created. S_3 increases the pressure of the inlet air, but also reduces its velocity to zero. Once the shockwave reaches the inlet side of the rotor, the AI port is closed. This results in a channel full of fresh air with zero velocity (Zone I). The channel is now at the same initial conditions as the beginning of the wave pattern, and is ready to begin the cycle again.

Once the wave pattern has been established, it is possible to calculate the port timings and other design variables. The port timings will largely be dependant on the time required for the shockwaves and expansion waves to travel across the rotor. The gas dynamics behind the operation of the wave disc are governed by the following set of equations [3]. Using these equations, it is possible to calculate the flow velocities and port timings for the wave pattern.

Shockwave relations:

$$\Pi_S = \frac{P_2}{P_1} \tag{1}$$

$$\frac{T_2}{T_1} = \Pi_S \left(\frac{\frac{\gamma+1}{\gamma+1} + \Pi_S}{1 + \frac{\gamma+1}{\gamma+1} \cdot \Pi_S} \right) \tag{2}$$

$$w = a_1 \sqrt{\frac{\gamma+1}{2\gamma}(\Pi_S - 1) + 1} \tag{3}$$

$$u_p = \frac{a_1}{\gamma}(\Pi_S - 1)\sqrt{\frac{\frac{2\gamma}{\gamma+1}}{\Pi_S + \frac{\gamma-1}{\gamma+1}}} \tag{4}$$

Where: 1 – conditions in front of the shock, 2 – conditions behind the shock, w – velocity of the shockwave, u_p – induced velocity of the flow behind the wave.

Expansion wave relations:

$$\frac{a_2}{a_1} = 1 \pm \frac{\gamma-1}{2}\frac{u_2 - u_1}{a_1} \tag{5}$$

$$\frac{T_2}{T_1} = \left(\frac{a_2}{a_1}\right)^2 \tag{6}$$

$$\frac{P_2}{P_1} = \left(\frac{a_2}{a_1}\right)^{\frac{2\gamma}{\gamma-1}} \tag{7}$$

$$\begin{cases} u_{head} = a_1 \pm u_1 \\ u_{tail} = a_2 \pm u_2 \end{cases} \tag{8}$$

Where: 1 – conditions in front of the wave, 2 – conditions behind the wave, w – velocity of the shockwave, u_{head} –velocity of the head of the wave, u_{tail} – velocity of the tail of the wave.

4.2 IMPROVED WAVE PATTERN

With the wave pattern presented in the previous section, the calculations involved are not too complex or time consuming, so they may be carried out by hand. However, in order to do this, that pattern has some major simplifications. A computer code was envisioned to solve for the wave pattern. This code reduces calculation time and is capable of solving more complex equations. This enabled the production of an improved wave pattern. The new pattern is more accurate and uses fewer simplifications than its predecessor.

The basic wave pattern calculated by the code is similar to the simple pattern presented in the previous section. The improved wave pattern is shown in Figure 18. It adds some significant changes to the gas/air interface and the low pressure portion of the rotor.

The first major enhancement consists of the change of speed of the shockwaves and expansion waves when they cross the gas/air interface. The waves move from a low temperature medium to a high temperature medium, or vice versa. Also, the exhaust gas has a different specific heat ratio, γ, than the air. From the aforementioned gas dynamics equations, the speed of the wave depends on both the temperature and the specific heat ratio of the air. In general, the waves will move at a higher velocity in the exhaust gas than in the air. This can be noticed on the wave pattern by the change in slope of the waves as they cross the gas/air boundary.

The second improvement on the wave pattern is a more accurate calculation of the position of the gas/air boundary. The flow within the rotor is mainly dependant on the shockwaves and expansion waves. Shockwaves induce the channel flow in the same

direction as they propagate. Expansion waves have the opposite effect. As a result, when any wave crosses the gas/air boundary, it should speed it up or slow it down. For example, when the second shockwave crosses the gas/air interface, it slows it down, since it is moving in the opposite direction than the boundary itself. This can be again seen by the change in slope of the boundary in the wave pattern. When this is taken into account, it produces a much more accurate prediction of the position of the interface.

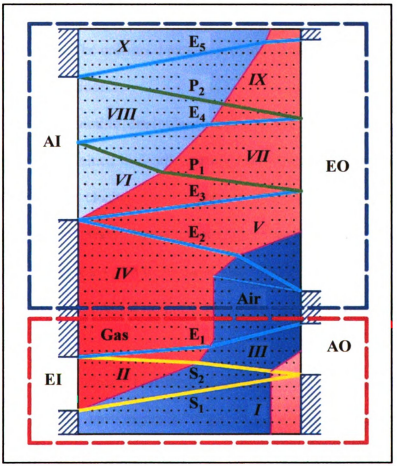

Figure 18. Improved wave pattern for a through-flow wave rotor

Using this more accurate prediction for the gas/air interface, it is possible to notice that in a majority of cases, the compressed air fails to fully exit through the AO port before it is closed. Therefore, in zone IV, when the channel is at rest between the AO

and EO ports, a portion of the channel is still taken up by fresh air. This air then exits the rotor through the EO port, in the low pressure section of the rotor.

A number of important changes were made to the wave pattern in the low pressure section of the disc. For the simplified pattern, all the reflected waves within the low pressure portion were ignored. When an expansion wave reaches a boundary, it may either reflect as an expansion or a pressure wave. In this pattern the reflections of the second expansion wave, E_2, are taken into account in order to improve the porting design in the low pressure part. The enhanced pattern provides better scavenging of the exhaust gas before the EO port is closed.

Due to the considerable dissimilarity between the two patterns, the improved wave pattern is again explained in detail, starting from Zone IV, where the channel is at rest between the AO port closing and EO port opening. As before, when the EO port opens, a strong expansion wave (E_2) is created, traveling to the inlet side of the rotor. Because this is a strong wave, both the head and the tail of the wave are taken into account. The AI port is not opened until the tail of the expansion wave reaches the inlet side of the channel.

When E_2 sees the closed boundary at the inlet side, it is reflected as a weak expansion wave (E_3). This wave expands the gas in the channel to a lower pressure, and also slows it down (Zone V). When E_3 arrives to the EO port, it is reflected as a pressure wave (P_1). The pressure ratio across the EO and AI ports is not large enough to create shockwaves. The first pressure wave travels across the channel, increasing the pressure of both the exhaust gas and air (Zone VI). It also has the effect of slowing down the flow, since it is moving in a direction opposite to the flow.

This process is repeated one more time, creating expansion wave E_4, pressure wave P_2 and Zones VIII and IX. The closing of the AI port is timed with the arrival of the last pressure wave (P_2) to the inlet side of the rotor. This creates the final expansion wave (E_5), which decelerates the flow in the channel to zero velocity (Zone X). When this final expansion wave reaches the outlet side of the rotor, the EO port is closed and the channel is completely at rest. This channel is then used at the beginning of the next cycle.

Multiple waves cross the gas/air interface in the low pressure portion. Each of these waves has the effect of reducing the speed within the channel. As a result, the gas/air interface is repeatedly slowed down, and may not be able to reach the EO port before it is closed. If this occurs, an amount of exhaust gas will remain in the channel after the wave pattern is complete, and the next cycle will not start with a clean channel full of fresh air.

That is the final important enhancement for the new pattern. It allows for recirculation to occur, if necessary. Therefore, the channel may begin the new cycle with the final portion taken up by exhaust gas. The exhaust gas then exits the rotor through the AO port. Depending on the design, it may not be possible to avoid this phenomenon, and some recirculation will occur regardless of the operating conditions chosen for the rotor.

4.3 1-D Design Code for Wave Disc

In order to solve for the wave pattern and port timings, a 1-D design code was developed at the MSU Turbomachinery Lab [28,29]. This code was developed using MATLAB for a wave rotor used to enhance a gas turbine engine. It was then possible to modify it to apply for a pressure exchange wave disc.

The 1-D design code requires a few inputs which need to be determined before it is executed. The inputs depend largely on the application for the wave rotor or wave disc that needs to be produced. The length of the channel is an important input parameter. This will depend on the overall size of the device. Also, the pressures and temperatures at the two inlets of the rotor have to be supplied. The desired pressures at the two outlets must also be given.

Among the outputs of the code, the most important are the port timings and the flow velocities along the inlet and outlet ports. The code also outputs mass flow rates and an ideal rotational speed for a wave rotor, but these results cannot be applied to the wave disc due to their different geometries. The flow velocities, however, can be used to determine the ideal angles for the inlet and outlet porting.

The port timings are used to determine the porting geometry for the wave disc. The wave pattern in the disc remains the same, so the port timings also remain the same. From these timings, it is possible to calculate the porting angles for the wave disc separately. In order to do this, a rotational speed must be assumed. In most cases, it is calculated from the number of cycles required for the disc. For example, if the disc has four cycles, all the porting angles must fit between 0° and 90°. Usually, though, it is best

to leave some space between different cycles on the disc, so the rotational speed is decreased slightly to allow this.

Furthermore, the code creates a plot displaying the wave pattern and velocities at the inlet and outlet ports. This allows for a quick, visual analysis of the results. Two sample operating points are given in Table 1, with their outputs shown in Figure 19. The output on the left shows a wave pattern without EGR, where the gas/air interface exits the rotor through the EO port. The output on the right shows a wave pattern with EGR, where the rotor is not fully scavenged. The exhaust gas exits the channels at the AO port at the beginning of the cycle instead.

Table 1. Sample operating points for 1-D design code, results shown in Figure 19

	Operating Point 1	**Operating Point 2**
L	0.093 m	0.093 m
P_1	0.98 bar	0.99 bar
P_2	2.40 bar	1.88 bar
P_3	1.80 bar	1.50 bar
P_4	1.02 bar	1.01 bar
T_1	300 K	300 K
T_3	1100 K	1100 K

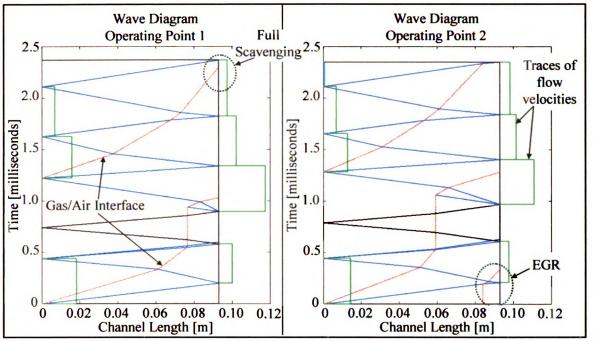

Figure 19. Wave pattern outputs for two operating points.
Left – Fully scavenged rotor. Right – EGR Present.

The wave pattern and porting design created by the 1-D code are a good starting point for numerical modeling. This preliminary design provides a good approximation for the wave pattern in the rotor. However, it still does not take into account important effects such as centrifugal forces and leakage. The preliminary design produced by the 1-D code needs to be simulated more accurately, improved, and validated.

4.4 WAVE PATTERN FOR INTERNAL COMBUSTION WAVE DISC ENGINE

The external combustion wave disc engine uses a pressure exchange wave disc, which can be designed by the code mentioned in the previous section. The internal combustion wave disc engine uses a completely different wave pattern. It was necessary to develop a separate wave pattern and 1-D code only to be used for an IC wave disc engine.

Only two ports are present in an IC wave disc engine: the air/fuel mixture inlet and the exhaust outlet. The wave pattern is designed to completely scavenge the rotor before a new cycle begins. No EGR should be present in the channel when combustion occurs. For the inlet, the mixing of the two fluids occurs before the inlet port, and is assumed to be of even, constant concentration. This fuel/air mixture is near atmospheric pressure. The exhaust outlet pressure is higher than the air inlet, but significantly lower than the combustion pressure.

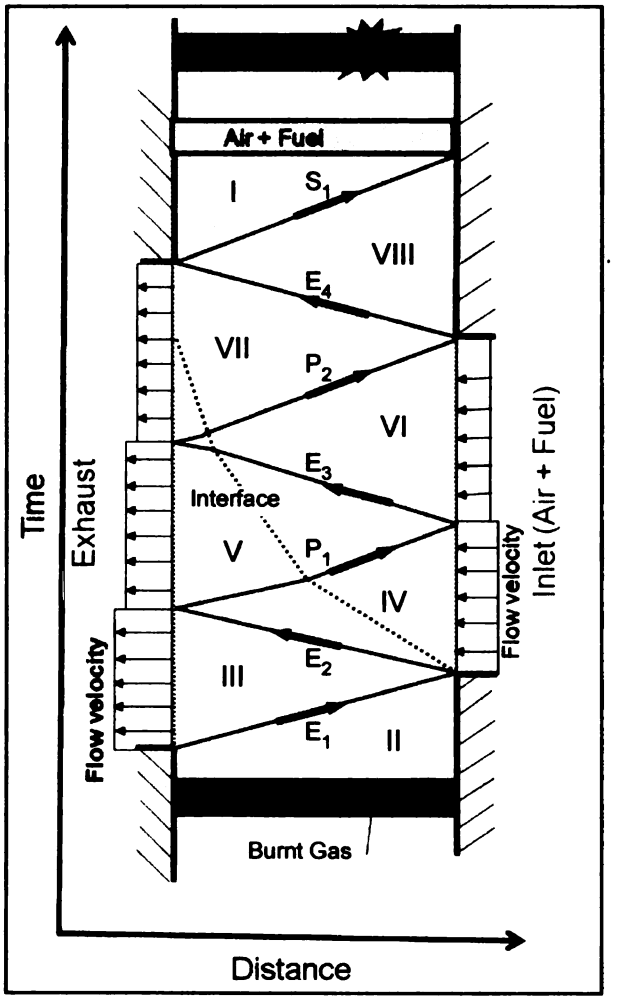

Figure 20. Wave diagram for a wave disc with internal combustion

The wave pattern developed is shown in Figure 20 and Figure 21. The first is shown in a relative reference frame. The horizontal axis represents the position within the

channel, and the vertical axis represents time. The second figure uses an absolute reference frame. The same wave pattern is presented, but shown for a radial wave disc. In this case, the shockwaves are curved, following the motion of the rotating channels.

The wave pattern begins after the combustion process. At this point, the rotor is filled with combusted gas with a through-flow velocity of zero. Furthermore, the channel is now at the highest temperature and pressure in the cycle (Zone II). The outlet side of the rotor is then opened to the exhaust port, which is at a lower pressure than the channel. This creates a strong expansion wave (E_1), which travels into the channel. The expansion wave produces two effects. First, it expands the gas in the channel to a lower pressure. Second, it induces a fluid flow in the direction opposite to that in which it is traveling. This forces the expanded combustion gas out of the channel (Zone III).

When the first expansion wave reaches the inlet side of the rotor, it is reflected as another expansion wave (E_2). At this time, the inlet port is opened, allowing the fresh air/fuel mixture into the channels. E_2 expands the exhaust gas to the same pressure as the inlet air. Both the expanded gas and the inlet air travel into the channel. The gas/air interface becomes visible in this area (Zone IV).

When E_2 reaches the open exhaust port, it is reflected as a pressure wave (P_1). This pressure wave compresses both the gas and mixture inside the channel, but also slows it down (Zone V). The pressure wave then reflects as an expansion wave on the open inlet side of the channel. This reflection process continues with the same effects until the exhaust gas is completely scavenged out of the rotor.

When the gas/air interface reaches the outlet side of the rotor, the channel is entirely filled with fresh air/fuel mixture (Zone VII). At this point, the last pressure wave

(P_2) is allowed to reach the inlet side of the channel. Once the pressure wave reaches the inlet and reflects as an expansion wave (E_4), the inlet port is closed, preventing any flow from entering the rotor. A low pressure area is created in the wake of the wave (Zone VIII).

At this point, compression is necessary to pressurize the air/fuel mixture to the conditions necessary for combustion. The exhaust port is closed when the last expansion wave reaches the outlet side of the channel. The sudden closure of the port forces the flow to come to a rest, which creates a strong shockwave (S_1). This shockwave moves through the channel, compressing the mixture and decelerating all the flow to a velocity of zero. The wave pattern is complete and the channel is at rest. It contains a compressed air/fuel mixture (Zone I). This mixture can then be ignited, increasing both the pressure and temperature of the channel (Zone II). This returns the channel to the conditions at which the wave pattern can begin again.

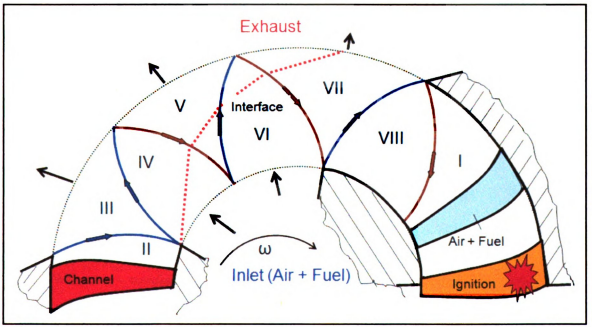

Figure 21. Wave diagram for an internal combustion wave disc shown in absolute reference frame

The biggest challenge with modeling this wave pattern concerns how to model the combustion process accurately. Combustion occurs in a constant volume, confined channel. It provides not only a temperature increase, but also a pressure increase. The fuel chosen was hydrogen. The combustion process was modeled using a constant volume adiabatic flame temperature calculation. The flame temperature calculation assumes complete combustion of the reactants, and is capable of calculating a flame temperature at rich, lean, or stoichiometric conditions. For the stoichiometric calculation, the following reaction balance is used:

$$H_2 + \frac{1}{2}(O_2 + 3.76N_2) \rightarrow H_2O + 1.88N_2 \tag{9}$$

The adiabatic flame temperature can be obtained from the first law of thermodynamics, simplified for an adiabatic, constant volume process. With no exchange of heat or work, the internal energy of the reactants must be equal to that of the products.

$$Q - W = \Delta U \tag{10}$$

$$U_r(T_i, P_i) = U_p(T_f, P_f) \tag{11}$$

This can be put in terms of enthalpy, keeping in mind the pressure rise occurring within the closed system.

$$H_r - H_p - V(P_i - P_f) = 0 \tag{12}$$

Using the ideal gas law, this can this can be further simplified to

$$h_r - R_i T_i = h_p - R_f T_f \tag{13}$$

Where: r – reactants, p – products, T_i – initial temperature of the reactants, T_f – adiabatic flame temperature.

The pressure rise caused by the combustion process is calculated using the ideal gas law. For a closed volume system, the equation is simplified to:

$$\frac{P_f}{P_i} = \frac{R_f T_f}{R_i T_i} \tag{14}$$

Where: i – conditions before combustion, f – conditions after combustion.

Using predefined enthalpy values for a range of temperatures [33], the adiabatic flame temperature can be calculated using an iterative numerical method. The lean and rich calculations are performed in the same manner, the only difference being the reaction balance that is used. Finally, the flame temperature is scaled with the mass of fresh air/fuel mixture in the channel. In this manner, if EGR occurs, the flame temperature is reduced to compensate for it.

Both the wave pattern and combustion process must be solved numerically. A MATLAB code was developed to automatically solve for the wave pattern, port timings, and combustion results. The code requires a set of input parameters from the user. The first is the length and height of the channels. The pressure and temperature of the inlet air/fuel mixture is necessary, and the desired outlet pressure for the exhaust gas may be specified.

After calculation, the code outputs a complete flow pattern, including complete port timings and velocities. The adiabatic flame temperature for combustion is solved, along with its corresponding pressure rise. The flow pattern is also displayed visually. An example is shown in Figure 22. This sample is created for the operating point given in Table 2. The output shows a wave pattern without EGR, where the rotor is fully scavenged at the beginning of each cycle.

Table 2. Sample operating point for internal combustion wave disc engine, result shown in Figure 22

	Operating Point
L	0.093 m
P_1	1.5 bar
T_1	300 K
P_2	1.01 bar

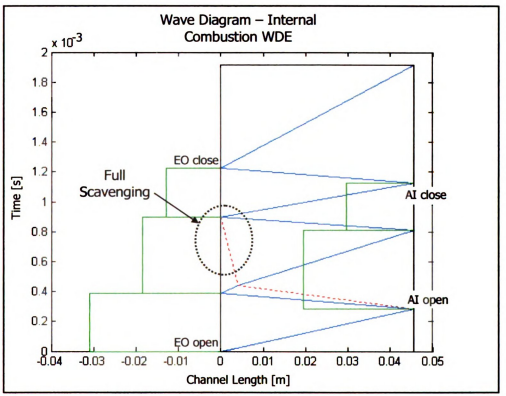

Figure 22. Wave pattern output for an internal combustion wave disc engine

CHAPTER 5: AUTOMATED WAVE DISC SIMULATION CODE

5.1 NUMERICAL SIMULATIONS OF WAVE DISCS

Numerical simulations are necessary to validate the results of the 1-D design codes. Computational Fluid Dynamics (CFD) software models the flow and wave patterns present in the disc. In order to work effectively, the 1-D algebraic codes do not take into account various processes that occur within the rotor. In order to confirm the results of the 1-D codes and progress in the design, the wave disc needs to be simulated fully using CFD software.

The simulations must take into account any important parameters that were not included in the 1-D code and might have an effect on the solution. This includes the effects of the secondary waves created by the pressure and expansion waves in the low pressure section of the disc. The centrifugal forces acting on the disc need to be taken into account, as they could provide to be helpful in scavenging the rotor. The CFD models also include a gap between the porting and rotor which allows for leakage. The algebraic code only allows for inlet and outlet velocities to be perfectly radial, while the CFD models allow the air to enter and exit the rotor at an angle. Backflow may be present at the inlet and outlet boundaries and should be taken into account. Viscous forces might have an effect on the design, as well as heat transfer through the channel walls. Finally, the 1-D code always assumes straight channels. The 2-D models may use curved channels to help the rotor extract energy from the flow. All of these effects are present within the 2-D CFD simulation, producing a much more realistic solution.

In addition to validating the 1-D algebraic code results, the results of the 2-D numerical simulations are analyzed and used to further improve the wave disc design. Most of the time, this produces changes to the design that need to be verified. These need to be modeled through a completely new simulation. Often multiple iterations are completed for a single design. The majority of the design changes lead to a change in its geometry, requiring the entire process for obtaining a solution to be repeated. This needs to be done even for the smallest changes in the geometry of the design. Completing a single simulation by hand, including the modeling, solving and post-processing, would require a few days. Using this method a complete wave disc design could take anywhere from weeks to months.

In order to improve and speed up the design process for the wave disc, a MATLAB code was developed to automate the numerical simulation process. The code is capable of performing a full simulation given a set of input matrices. The input matrices define geometric parameters, meshing parameters, solver settings, and boundary conditions for a single simulation. The code then creates and meshes the geometry, sets up and runs the simulation, and completes some post-processing.

MATLAB is used to interface with GAMBIT 2.3 and FLUENT 6.2. The MATLAB code passes commands to both programs through the use of journal files. These files are text files that contain either GAMBIT or FLUENT specific commands. The journal files are created every time the code is run, with different commands depending on the code's input variables. MATLAB then activates the required program and gives it a specific journal file to run. The program then runs through all the commands in the journal file and quits. In this manner, MATLAB is used to create and

mesh the geometry and domains in GAMBIT. It then is used to setup and run the simulation in FLUENT, and post-process the FLUENT results.

5.2 GEOMETRY

The initial step to simulating a wave rotor is defining the geometry. GAMBIT 2.3 was used to perform this task. GAMBIT is a pre-processing program used mainly for FLUENT. Its purpose is to create the geometry, mesh, and domains that will be used by the CFD solver. The geometry in this program is defined as a series of vertices (points), connected by edges (lines or curves), which in turn make up faces. In order to create the geometry, the MATLAB code is required to give GAMBIT the commands to create these vertices. MATLAB also has to give GAMBIT the commands to connect the lines correctly and create the faces.

An algebraic code was created in MATLAB to calculate the geometric points required by GAMBIT. The code has a certain set of input variables that are used to calculate the shape and size of the wave disc porting and of the individual channels. A list of the input variables required to create the porting geometry is given in Table 3 and shown schematically in Figure 23. The list of input variables required to create the channel geometry is given in Table 4 and shown in Figure 24 and Figure 25.

The MATLAB code is flexible in order to accommodate for many different designs. By changing the input variables, the geometric points required by GAMBIT are be recalculated to match. This in turn changes the edges and faces of GAMBIT to match the changes in the inputs. The input variables were chosen based on experience with wave disc design.

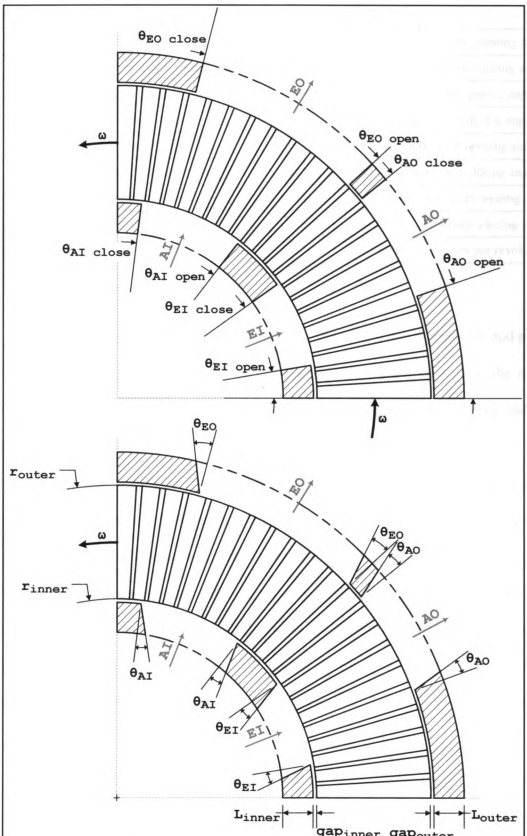

Figure 23. Schematic of the input variables necessary for the porting geometry

Table 3. Input variables necessary for generation of porting geometry

r_{inner}	Inner radius of rotor
gap_{inner}	Size of gap on rotor inner radius
L_{inner}	Length of porting on inner radius
r_{outer}	Outer radius of rotor
gap_{outer}	Size of gap on rotor outer radius
L_{outer}	Length of porting on outer radius
θ_{EI}	Angle of exhaust inlet porting
θ_{AI}	Angle of air inlet porting
θ_{AO}	Angle of air outlet porting
θ_{EO}	Angle of exhaust outlet porting

$\theta_{EI\ open}$	Exhaust inlet port opening angle
$\theta_{EI\ close}$	Exhaust inlet port closing angle
$\theta_{AI\ open}$	Air inlet port opening angle
$\theta_{AI\ close}$	Air inlet port closing angle
$\theta_{AO\ open}$	Air outlet port opening angle
$\theta_{AO\ close}$	Air outlet port closing angle
$\theta_{EO\ open}$	Exhaust outlet port opening angle
$\theta_{EO\ close}$	Exhaust outlet port closing angle
c	Number of cycles per revolution

For the porting geometry, the input variables define the size of the rotor and ports, the opening and closing of the ports, and the angles of the ports relative to the radial lines. It also allows the user to specify gap size between the rotor and porting and the length of the ports themselves.

The user may also choose any number of cycles per disc, *c*, starting from one. If only one is chosen, there will be one cycle per full revolution using the defined porting angles, and the ports will remain closed for the rest of the revolution. If two cycles are chosen, the cycle will repeat after 180°. For four cycles, there will be one every 90°. For rotors that have more than one cycle per revolution, each cycle will repeat the exact same geometry and wave pattern as the others. As a result, only one of the cycles needs to be modeled for CFD. This helps reduce the computation time required to complete the simulation.

The channel geometry is defined in a different manner than that of the porting. The channels may be straight or curved, and may take on any curvature required. The channel shape is defined by a set of points spanning the length of the rotor. Each of these

points is at a dimensionless distance from the inner edge of the rotor. Each point also has a relative angle from a horizontal reference which is used to define the curvature. Since GAMBIT uses a NURBS curve interpolation to create the channel walls, the more points are defined, the more accurate the GAMBIT model will be to the desired curve. The user may input as many points as necessary, with a minimum of two. Another input variable is the total number of channels in the rotor. From this variable, the size of the channel unit, $\Delta\Phi$, which consists of a single channel and a single wall, can be calculated. Within the channel unit, the user can specify how much of the unit is taken up by the channel, φ, and how much is taken up by the wall. This needs to be done for every point specified for the channel curvature.

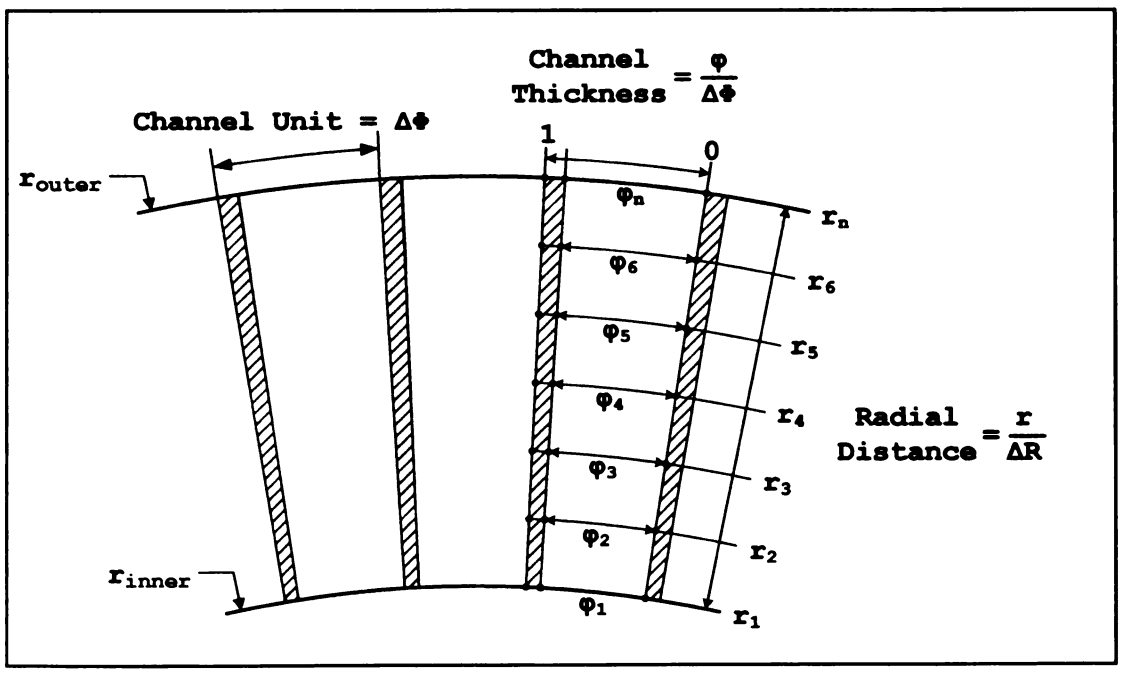

Figure 24. Schematic of the input variables necessary for a straight channel

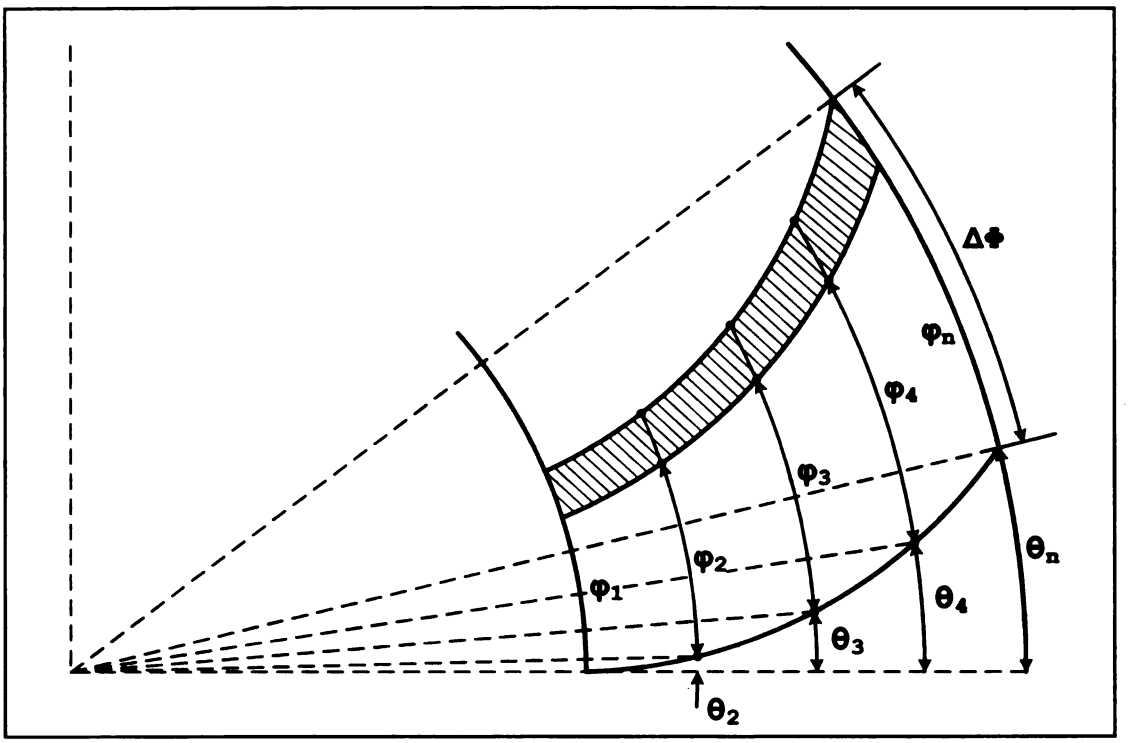

Figure 25. Schematic of the input variables necessary for a curved channel

Table 4. Input variables necessary for generation of straight and curved channels

$N_{channels}$	Number of channels in full rotor	
r/ΔR	**θ**	**φ/ΔΦ**
r_1	θ_1	φ_1
r_2	θ_2	φ_2
r_3	θ_3	φ_3
r_4	θ_4	φ_4
r_5	θ_5	φ_5
...	...	...
r_{N-1}	θ_{N-1}	φ_{N-1}
r_N	θ_N	φ_N

5.3 MESH

Once the geometry is defined, a mesh needs to be created. GAMBIT is used to create the mesh. Several options are available for meshing. However, in order for the mesh to adapt to multiple, different designs, it was necessary to use a structured grid with a fixed number of mesh points. Using any other type of meshing option would not be flexible enough to work for multiple types of geometries. This can be seen by comparing Figure 26 with Figure 27. The first mesh is a structured grid, in which the mesh size and shape adapts to the wave rotor features. It aligns to the shape of the port, which is angled, and to the shape of the channel, which is straight. The mesh in the second figure uses a semi-structured grid, in which the grid attempts to align with the geometry, but does not have a constant number of mesh points. The uneven mesh points cause the grid to become very skewed in certain areas, in this case in the gap between the rotor and porting. This type of mesh will produce numerical errors during the simulation process.

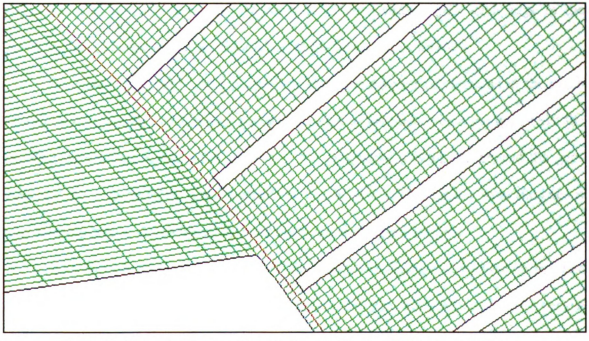

Figure 26. Close-up of inner gap for a structured grid, aligned with geometric features

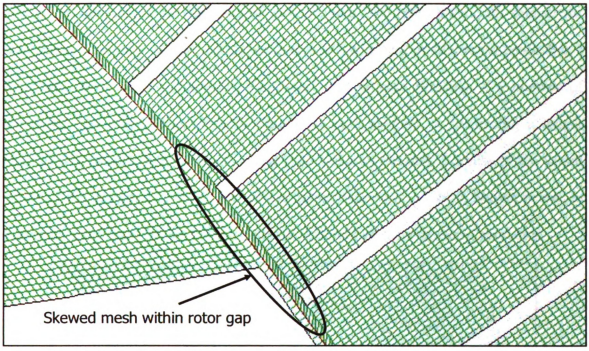

Figure 27. Close up of inner gap for a semi-structured grid, with skewed mesh within gap

In order to avoid meshing errors, the grid is made up of quadrilateral elements, aligned with the porting and channels. With any design variations, the mesh would adapt and re-align to the new geometry. In order to achieve such a grid, each edge in the geometry has to be meshed individually before the faces can be meshed.

To reduce the computational solution time, the number of elements in the mesh should be minimized. The limiting factor is the size of the gaps. Since the gaps have the smallest dimensions in the entire geometry, the grid points within and around the gaps may only be as large as the gaps themselves. As the grid moves further from the gaps it may become larger, which occurs in both the channel and port meshes.

The number of mesh elements and their size will change depending on the size and shape of the wave disc. In order to compensate for this, the user has control over the number of radial and tangential grid points to be used for meshing. The number of radial

grid points determines the thickness of each element. The more points, the thinner the elements will become. A rotor with more cycles will take up a smaller radial space than a rotor with fewer cycles, requiring less radial grid points. Similarly, the number of tangential grid points determines the length of each element. A rotor with a longer channel will require more points than one with a shorter channel. Because of the varied nature of the designs, it is up to the user to define these two variables. Shown below, in Figure 28 and Figure 29, are two examples of different grids on the same geometry.

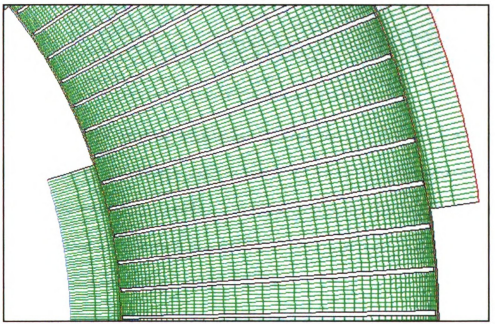

Figure 28. Close-up of high pressure zone with a coarse mesh, with 270 radial mesh points and 50 tangential mesh points

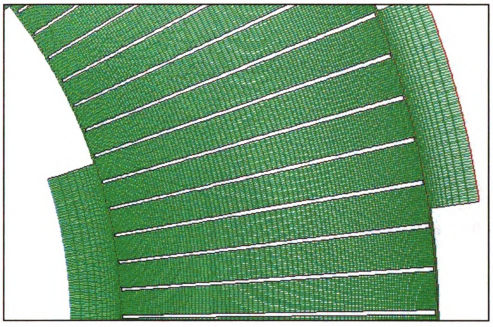

Figure 29. Close-up of high pressure zone with a fine mesh, with 540 radial mesh points and 100 tangential mesh points

The last step to meshing is defining the domains and boundaries to the mesh. Each edge needs to be defined as a wall, an inlet or an outlet. The fluid zones of the rotor, gaps and ports also need to be specified. The edges that connect the rotor fluid zone to the gap fluid zones need to be defined as interfaces. Also, the top and bottom edges of each gap need to be linked and defined as periodic edges.

Once the meshing is complete and the boundaries and domains are defined, the mesh is exported and saved. An example, shown in Figure 30, labels all the boundaries in a 4-cycle wave disc. The single cycle occupies 90° of the rotor. For this example, the mesh is coarse, and the geometry has both angled porting and curved channels. The full wave disc is shown in Figure 31. The completed mesh can then be imported and used by the CFD solver.

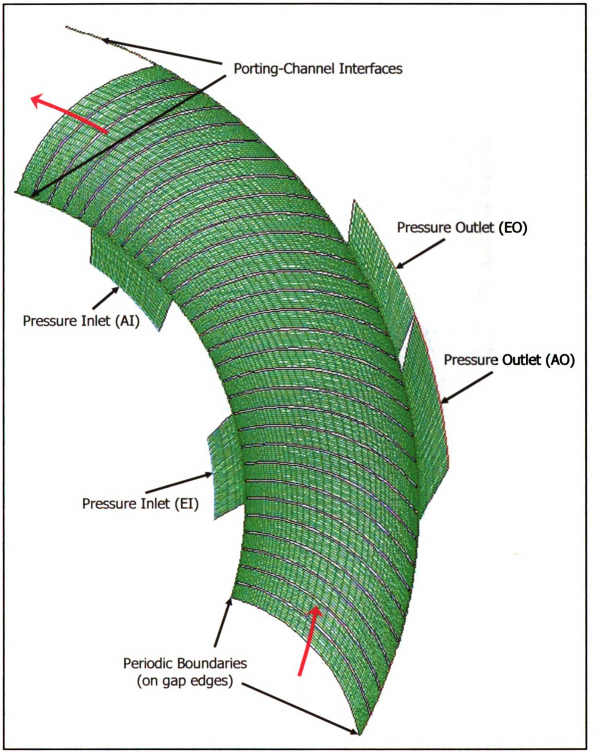

Figure 30. Complete mesph for a 4-cycle wave disc with curved channels and angled porting

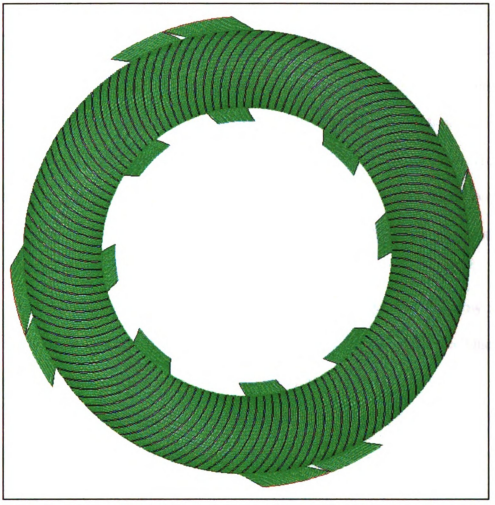

Figure 31. Full model of the 4-cycle wave disc with curved channels and angled porting

5.4 PRE-PROCESSING SETUP

The CFD software used to model the flow and wave patterns in the rotor is FLUENT 6.2. It is a commercial package that has proven to accurately model the unsteady flow created by the wave disc. Its 2-D, double precision solver is used to run the simulations. When a mesh is imported into FLUENT, the simulation needs to be pre-processed in order to run. The MATLAB code created takes care of the solver settings and initializes the solver automatically.

For wave disc simulations, the segregated, implicit solver was chosen. The segregated solver was chosen in order to avoid numerical errors during the transient start-up of the wave disc. During initialization, the entire rotor is at ambient conditions, while the exhaust inlet and air outlet ports are at very high pressures. The high pressure at the air outlet creates shockwaves that induce the flow from the port into the rotor. However, this is an outlet port, so it causes backflow to occur across the pressure outlet boundary. The solver needs to allow backflow to occur. After enough cycles, the transient waves will die out and the normal wave pattern will control the flow.

The coupled solver does not handle this problem correctly. The backflow through the pressure outlet boundary is at a much lower velocity than it should be. Due to the error in backflow velocity, the port air does not flow into the channels as it should. Instead, the radial velocity around the outer radius of the rotor is very small, while the tangential velocity matches the tip speed of the rotor. This results in a numerical pressure error in that region. The high tangential velocity, combined with the erroneously low radial velocity, creates a stagnation point on the trailing edge of the air outlet port. This increases the pressure in that region to unrealistic values. This is illustrated in Figure 32. In the region where backflow should occur, the numerical error causes the pressure to increase drastically, and is an order of magnitude larger than the pressures within the rest of the model. The radial velocity contour also shows that backflow is not occurring within the channels. This problem does not occur with the segregated solver, which calculates the backflow correctly.

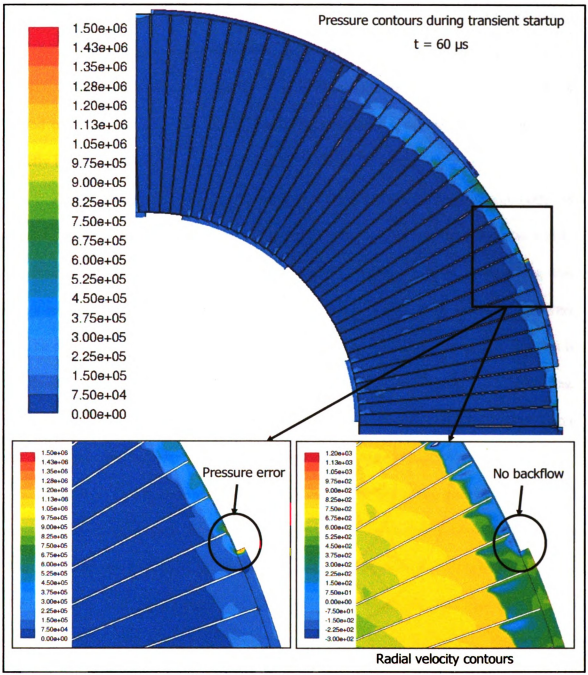

Figure 32. Numerical error present in coupled solver during transient start-up

The implicit and explicit solvers both work effectively for this type of problem [16, 18]. The implicit solver requires a fixed time-step, and completes multiple iterations between each step. The explicit solver uses an adaptive time step, and does not iterate between each step. However, the explicit solver requires a smaller time step than the

implicit, and the step size changes continually. If the program is run for a set number of iterations, there is no way to calculate or guess how much simulation time would have passed. Consequently, it would not be possible to program the simulation to run for a set period of time. The implicit solver was chosen because it allows the code to specify exactly how much time needs to pass in the simulation.

An inviscid solver was chosen for the automated code. The 1-D design code does not take viscous forces into account, so the simulation should match in order to validate the design. In addition, the size of viscous forces will depend on the scale of the rotor. Large rotors will see very limited and negligible viscous effects, while micro-scale rotors will be more affected. Even then, the effect of viscous forces will not be as large as for steady-state turbomachinery [15]. In order to complete the design, an inviscid approach should be taken. If necessary, the viscous forces should be added on the very last step of the design process, in order to verify that the design will still be effective.

The MATLAB code is then used to set up the boundary conditions. The code requires a set of user input variables which are used to set the inlet and outlet conditions. The rotational speed of the rotor is also an input. A complete list of inputs is shown in Table 5. The periodic interfaces are linked together automatically. The wave disc is modeled without heat transfer occurring between the walls. In most cases, this should not affect the solution, but should be confirmed once the design is complete.

Table 5. Input variables necessary for FLUENT pre-processing setup and simulation

grid unit	Specify units for geometry
P_{ref}	Reference pressure (atmosphere)
ω	Radial velocity of rotor
Δt	Simulation time step size
$\Delta t_{iterations}$	Maximum number of iterations per time step
N_{cycles}	Number of full cycles to be simulated

P_{EI}	Pressure of exhaust inlet port
T_{EI}	Temperature of exhaust inlet port
P_{AI}	Pressure of air inlet port
T_{AI}	Temperature of air inlet port
P_{AO}	Pressure of air outlet port
T_{AO}	Temperature of air outlet port
P_{EO}	Pressure of exhaust outlet port
T_{EO}	Temperature of exhaust outlet port

5.5 SIMULATION

In order to begin the simulation, the entire rotor is initialized at the air inlet temperature and pressure. Each port is then patched at its corresponding temperature and pressure. Since the exhaust inlet port is at a higher pressure than the rotor channel, shockwaves will propagate into the channels, as is expected. However, the air outlet port is also patched at an even higher pressure. Due to this, shockwaves will propagate into the channel in the opposite direction of the flow. This creates an initial backflow, during the transient startup of the rotor.

After a certain amount of time, the transient startup of the rotor ends. At this point the wave disc is operating at steady state. The process is still unsteady, but the wave pattern, inlet and outlet conditions do not change with time. It is therefore possible to claim that the rotor as a whole is operating at steady state. The time required to reach steady state depends on the size and speed of the rotor.

An implicit solution was chosen for the iterative method, which requires a fixed time step size, Δt. The size of the time step was left as an input for the user. The smaller

the time step is, the longer it will take to reach a solution. However, the time step cannot be chosen at random. It must be less or equal to a maximum value in order for the solution to converge. The maximum value of the time step can be determined through the Courant-Friedrichs-Lewy (CFL) criterion [4,16]. This criterion states that the time step size, Δt, cannot be grater than the time required for a sound wave to travel between two adjacent grid points. Since the size of the grid changes within the rotor and porting, this criterion should be valid for all of the grid points in the mesh. Therefore, the limiting grid points are those closest together, which occur at the gaps between the rotor and porting. The grid size will change depending on the user inputs, so it was determined that the user should calculate and input the time step size to be used in the simulation.

In order to account for the transient startup the simulation needs to be run until the rotor reaches steady state operation. Since the flow within the rotor is unsteady it is not possible to use the residual values from FLUENT to determine when the simulation is complete. It is therefore necessary for the user to input the number of full cycles to be completed before the rotor reaches steady state, N_{cycles}. The code then calculates the number of total time steps required to complete the simulation, $N_{solution}$, using Equation (15). This depends on the rotor speed, ω, the number of cycles per revolution, c, and the time step size, Δt, all of which are input variables defined by the user.

$$N_{solution} = \frac{2\pi N_{cycles}}{c\omega\Delta t} \tag{15}$$

The following figures illustrate the transient start-up and steady-state operation of an example wave disc. The first figure shows the initial pressures for a wave disc and porting. The second figure shows the pressure contours of the rotor soon after the

simulation is started. The shockwaves moving into the channel from the air outlet porting can be seen clearly. The next figure is still within the transient start-up, but the wave pattern has begun to develop. The last two figures show the pressure contours after six full cycles. The wave pattern in both figures is clearly defined and does not change with time. For most cases, the rotor usually reaches steady-state before ten full cycles.

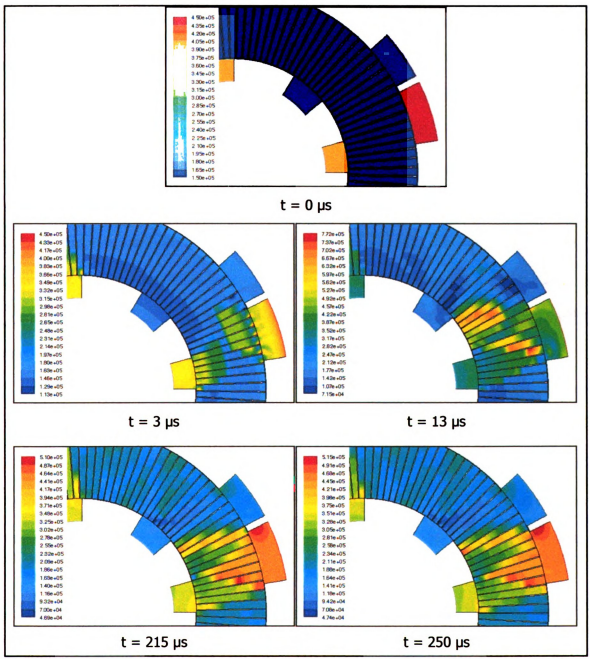

Figure 33. Wave disc pressure contours during initialization, transient start-up, and steady-state operation

5.6 POST-PROCESSING

Most of the post-processing may be done by the user once the code has completed the simulation. In this manner, the user can choose what to display and cater the output to his liking. The MATLAB code performs some post-processing functions before it allows the user access to the FLUENT solution files. Most of these functions are involved with the display features in FLUENT. The code automatically sets and saves the correct view for contour and vector plots. Also, if the rotor has more than one cycle per revolution, the code sets the periodic repeats for the rotor so that the full rotor can be seen when plotting.

Wave disc operation is unsteady, so it is common to create videos of the unsteady wave pattern in the disc for analysis. The videos give a better idea of the wave pattern and timing in the rotor. However, the video generation tool provided by FLUENT is very tedious and time-consuming. It is very prone to errors and often the output is not functional. Making the videos also requires large amounts of disc space. As a result, a separate MATLAB interface was developed with the purpose to quickly and easily produce videos of the wave pattern within the rotor.

The video post-processing interface has the capability of creating videos of any 9unsteady process within FLUENT. The videos are created from the contour plots for each time step within the desired time frame. The contour plots may be of a variety of properties available to FLUENT. In order for the code to work, the user must have all the case and data files for the time steps that are to be included in the video. FLUENT may be set up to save these files automatically as it runs a simulation.

The MATLAB code has a graphical user interface that allows the user to specify which files the video should be created from, what properties need to be recorded, the

range of values for each of those properties, and the time frame of the video. The interface is shown in Figure 34.

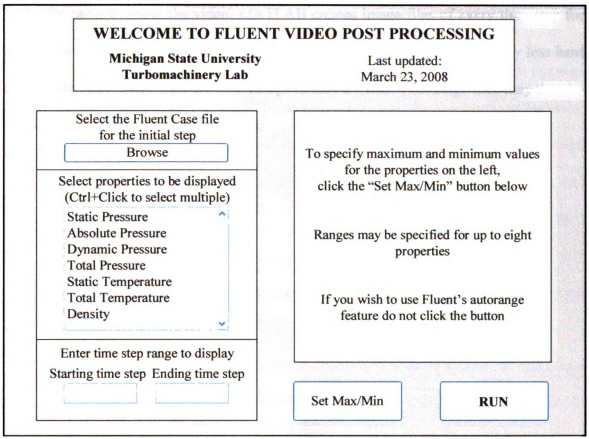

Figure 34. Graphical user interface for FLUENT post-processing interface

The user may define specific ranges for the properties selected, or use FLUENT's auto-range feature, where it automatically calculates the maximum and minimum values for each property. However, the auto-range feature in FLUENT has the drawback that the scale within the video will change every time step. This may result in confusing video patterns, where the colors and range in the plot change continuously. In most cases, it is preferable to create a first video using the auto-range feature. This video will allow the user to see what the maximum and minimum property values for that plot should be. The user may then create a second video with a specified, fixed range. In this manner, the

colors and range will remain the same throughout the video, making it much easier to view and understand.

In order to make the video, MATLAB creates image files of every time step for each property necessary. It saves these files in JPEG format, in order to occupy less hard drive space. The image files are then complied into a video. The image files may then be deleted after the video has been created.

CHAPTER 6: DESIGN METHODOLOGY AND RESULTS

6.1 DESIGN METHODOLOGY

The 1-D design code reported in Chapter 4 and the 2-D simulation code reported in Chapter 5 are necessary for the implementation of a new design methodology for radial wave discs. Previously, the development process was largely based on a single design calculated from the governing equations presented in Chapter 4. The wave pattern was simplified with assumptions in order to simplify the calculations. The design would then be modeled using CFD software, only to validate if it was feasible or not. Usually, only small adjustments would be made using the simulation results. This was due to the long time required to model and solve each design.

The new software developed allows the modeling and simulation to be completed in much less time. As a result, this process may be repeated numerous times, in order to improve the final solution and produce the best design possible. The new methodology takes advantage of this fact.

A flowchart for the new design methodology is presented in Figure 35. The first step is to develop the initial concept. This includes the operating pressures and temperatures for the wave disc its overall dimensions. This is largely dependant on the application for the new disc. Once that initial concept is set, the 1-D design code is used to create a preliminary design. From this design the necessary parameters for the 2-D simulation code can be extracted. This is a required step, since the 2-D code requires a more developed design than the initial concept required by the 1-D code.

The 2-D simulation code is then executed, and the results are analyzed. From this analysis, some design changes are recommended, and the design parameters are modified to reflect these changes. The new parameters are then executed once more by the 2-D code, and the results are again analyzed. This step is repeated as many times as necessary until it produces a satisfactory design that does not require any more changes. Once this design is agreed upon, the last possible step is the creation of a prototype for testing and final validation.

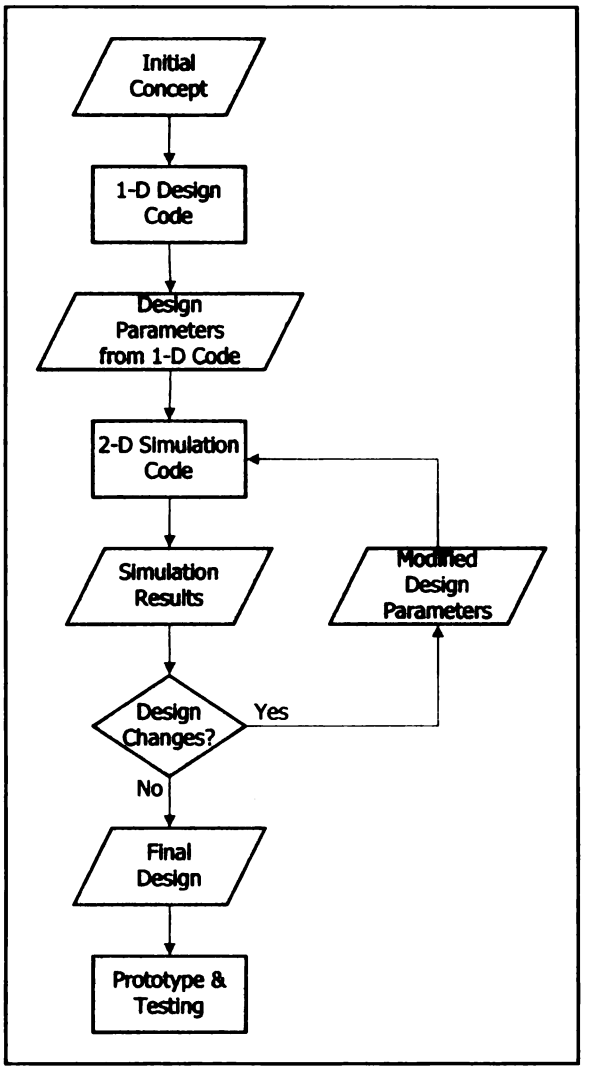

Figure 35. Flowchart of design methodology

6.2 NUMERICAL COMPARISON AND VALIDATION OF WAVE PATTERNS

The design methodology and numerical simulation code were used to study the effectiveness of the wave patterns developed for pressure exchange wave rotors. The two wave patterns presented in Chapter 4 were tested and the results were used to develop a more effective wave pattern and porting geometry. This process was completed for a millimeter-scale wave disc, to be used for second stage compression in a wave disc engine or gas turbine engine. The general geometry and operating conditions for this application are given in Table 6.

Table 6. General geometry and operation parameters for numerical comparison of wave patterns

Geometry Parameters	
r_{inner}	5 mm
r_{outer}	8 mm
gaps	0.03 mm
c	4 cycles/revolution

Operating Conditions	
N	350000 rpm
P_{EI}	400000 Pa
T_{EI}	1589 K
P_{AI}	150000 Pa
T_{AI}	435 K
P_{AO}	450000 Pa
T_{AO}	542 K
P_{EO}	162000 Pa
T_{EO}	1500 K

For the purpose of this analysis, three simulations were completed. The first simulation uses the porting geometry produced by the simple wave pattern. The second simulation uses the geometry produced by the 1-D MATLAB code using the improved wave pattern. The last iteration uses the results from the two previous analyses to create a final, improved design. A complete set of geometric parameters and operating conditions are given for each simulation in the Appendix.

The first simulation presented is modeled using the porting geometry calculated by the simplified wave pattern. The porting angles calculated are given in Table 7. The simulation results are presented in Figure 36. The results are presented in the form of pressure and temperature contours for one cycle in the wave disc, once it is operating at steady-state.

The pressure contours are used to display the wave pattern, while the temperature contours are used to display the gas/air boundary and the flow of each fluid through the rotor. From the pressure contours, it is possible to identify the shockwaves and expansion waves in the rotor by the sudden changes of pressure within the channels. The shockwaves create a very sudden and well defined boundary, while the expansion waves create a more gradual change of pressure.

From the temperature contours, it is possible to see the gas/air interface. It is marked by a sudden increase in temperature. The high temperature exhaust gas and low temperature air do not mix, creating a visible boundary between them. The motion of the interface also indicates the velocity of the flow within the channel. EGR may be noticed if high temperature exhaust gas remains in the rotor after the EO port closes. The EGR gas continues to rotate with the channels until the AO port opens in the next cycle.

Table 7. Porting angles calculated using simple wave pattern

$\theta_{EI\ open}$	0°
$\theta_{EI\ close}$	16°
$\theta_{AI\ open}$	39°
$\theta_{AI\ close}$	58°

$\theta_{AO\ open}$	9°
$\theta_{AO\ close}$	26°
$\theta_{EO\ open}$	28°
$\theta_{EO\ close}$	42°

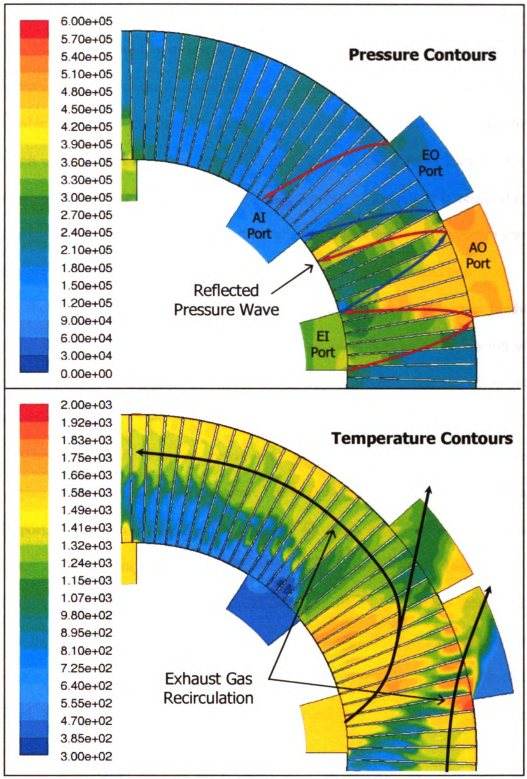

Figure 36. Pressure and temperature contours for a wave disc using the simple wave pattern

The pressure contours in Figure 36 show a clearly defined wave pattern. The first two shockwaves and the first expansion wave are all present in the high pressure portion of the disc. At the end of the AO port, it is also possible to identify an additional pressure wave which was not expected from the wave pattern. This wave is created by the reflection of the expansion wave at the AO port. In the original wave pattern, this port should close at the moment the expansion wave reaches it. Instead, it is open when the expansion wave reaches the outlet side of the channel, reflecting it as a pressure wave. It is therefore necessary for the AO port to close sooner, to avoid this reflection.

The low pressure portion of the wave disc follows the wave pattern as predicted. After the closing of the AI port, it is possible to see some very weak expansion waves traveling across the channel. These waves are mostly negligible and die out before the cycle begins again.

The temperature contours prove that this wave pattern is not effective at scavenging the exhaust gas from the rotor. The high temperature gas enters the rotor at the EI port, and travels across the channel to the EO port. This is seen from the gas/air boundary. However, only a portion of the exhaust gas leaves the rotor though this port. Approximately half the channel remains filled with exhaust gas, which then continues onto the next cycle and exits the AO port. This indicates that the EO port needs to remain open for a longer time and that the low pressure portion of the wave pattern needs to be modified, to reduce the EGR. The improved wave pattern calculated by the 1-D design code should negate this issue.

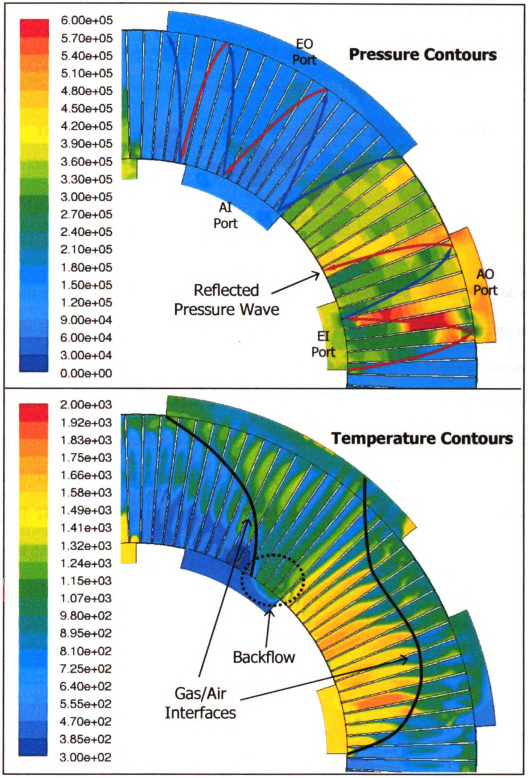

Figure 37. Pressure and temperature contours for a wave disc using the improved wave pattern

The second simulation was carried out using the porting geometry developed using the 1-D design code and improved wave pattern. The porting angles calculated are given in Table 8. The simulation results are presented in Figure 37.

Table 8. Porting angles calculated using 1-D design code and improved wave pattern

$\theta_{EI\ open}$	0°
$\theta_{EI\ close}$	19°
$\theta_{AI\ open}$	47°
$\theta_{AI\ close}$	76.5°

$\theta_{AO\ open}$	4.5°
$\theta_{AO\ close}$	23.5°
$\theta_{EO\ open}$	39°
$\theta_{EO\ close}$	85°

In the pressure contours for this geometry, the two initial shockwaves in the cycle are easily identified. However, the pressure profiles in the high pressure portion are not as well defined as those for the simple wave pattern model. In Zone III, between the second shockwave and the first expansion wave, the pressure in the channel drops significantly. The AO port opens too early, before the first shockwave can reach the outlet side of the channel. This creates an expansion wave that decreases the pressure in the channel in Zone III. The AO port must be opened at the exact time the shockwave reaches it in order to avoid this effect.

The extra reflected pressure wave that was seen in the previous simulation is also present in this one. Again, the AO port closes too late, reflecting the expansion wave as a pressure wave. The rest of the wave pattern matches the algebraic prediction for the low pressure portion of the disc.

The temperature contours for this geometry show a minimal amount of EGR. At the end of the cycle, the channel is mostly filled with air. However, the gas/air interfaces are not as clearly defined for this model as for the simple wave pattern model. The unexpected expansion waves present in the high pressure zone try to induce the flow in

the opposite direction than the shockwaves. These opposing forces allow the two fluids at the gas/air interface to mix, so the boundary is not as clearly defined. However, the majority of the exhaust gas in the channels is released through the EO port, with only a minimal amount remaining in the channel during the next cycle.

The temperature contours also show an area of unexpected backflow at the beginning of the AI port. The expansion wave that is created at the opening of the EO port should induce the flow into the channels. Expansion waves travel trough the channel at a relative speed equal to the speed of sound of the fluid within it. Due to the incorrect port timing in the high pressure part, the channel has a large amount of low temperature air present at the moment this expansion wave is created. This slows down the expansion wave, so it does not reach the AI port at the time it opens. Without the expansion wave, the flow is not induced into the channel, but instead flows out into the port.

The final iteration of the wave pattern is developed by combining the results from the previous two simulations. For the high pressure portion of the disc, the porting is returned to the geometry developed from the simple wave pattern. This geometry predicted the opening of the AO port more accurately, eliminating the unwanted expansion waves in the high pressure portion of the disc. Additionally, the time during which the AO port remains open is reduced. In this manner, the reflected pressure wave at the end of the high pressure zone is removed.

The low pressure portion of the rotor uses the same geometry developed from the improved wave pattern. This takes advantage of the improved scavenging properties of the second simulation. Figure 38 presents the simulation results for this geometry, the porting angles of which are given in Table 9.

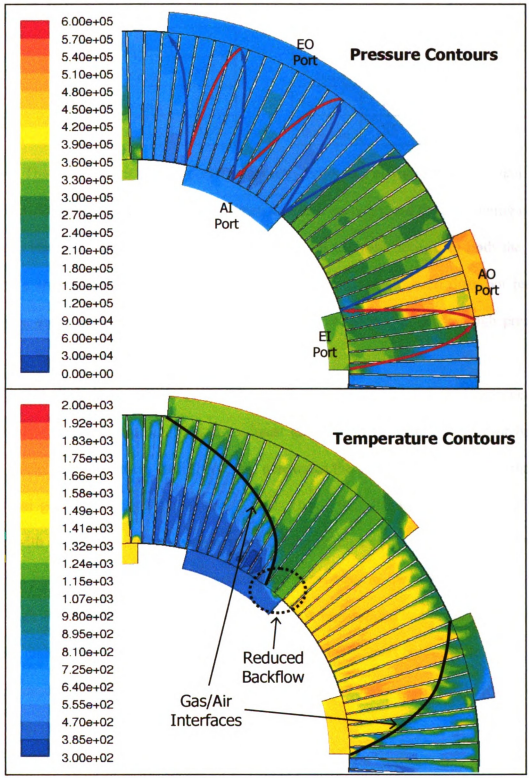

Figure 38. Pressure and temperature contours for a wave disc using final wave pattern iteration

Table 9. Porting angles determined for final wave pattern iteration

$\theta_{EI\ open}$	0°
$\theta_{EI\ close}$	16°
$\theta_{AI\ open}$	47°
$\theta_{AI\ close}$	76.5°

$\theta_{AO\ open}$	9°
$\theta_{AO\ close}$	23°
$\theta_{EO\ open}$	39°
$\theta_{EO\ close}$	85°

The final design for the porting geometry proves to be more effective than both previous designs. The wave pattern has been modeled correctly and the scavenging of the rotor is ideal. The shockwaves and expansion waves are well defined in both the high pressure and low pressure portions of the pressure contours. Zone III does not have a pressure drop, so the timing of the AO port is correct. At the end of the high pressure portion, there is no significant reflected pressure wave.

The temperature contours for this geometry show the important improvement achieved with this last design. All the exhaust gas is scavenged out of the rotor before each cycle. The gas enters the EI port and penetrates the channels much further than in the other geometries. By the time the AO port closes, the channel is almost completely filled with exhaust gas. In the same manner, all the exhaust gas exits the rotor, and when the EO port closes the amount of exhaust gas remaining in the channel is negligible. Although some mixing of the fluids still occurs, it is very limited and the gas/air interface is very clear. Finally, the outflow at the beginning of the AI port continues to be present. However, it is much reduced from the previous simulation, and does not affect the operation of the disc.

One final simulation was performed in order to validate the final wave pattern developed. In the three simulations presented previously, an inviscid solver was used. The wave patterns calculated in Chapter 4 all use the assumption of inviscid flow. It is

simpler to begin the design of the wave disc by ignoring viscous effects, in order to develop an effective porting design. Once this design has been reached, though, the result should be validated using the viscous solver in FLUENT. This is even more important at small scales, where the size of the viscous boundary layer will be more significant than for large rotors. The simulation results shown in Figure 39 were obtained using a laminar, constant viscosity model for the final porting geometry developed above.

The pressure contours for this simulation show the exact same pattern as the inviscid results. The temperature contours from the two simulations are very similar, but a viscous boundary layer can be seen at the walls of each channel. The viscous forces do not have a large effect on the operation of the wave disc. The rotor is still fully scavenged by the end of each cycle. However, with the viscous model, the gas/air interface reaches the outlet side too soon, and some exhaust gas is leaving the rotor through the AO port. Although this also occurred in the inviscid model, it was minimal. This is not ideal, but may be prevented by closing the AO port sooner.

Additionally, the velocity throughout the rotor has been reduced slightly by the viscous effects. Table 10 contains the mass-flow averaged velocity magnitudes at the inlets and outlets for both the inviscid and laminar simulations. As expected, the viscous simulation has consistently lower values.

Table 10. Comparison of velocity magnitudes at the inlets and outlets of the inviscid and laminar models

Inviscid Model Velocity Magnitudes	
Air Inlet	115.99 m/s
Air Outlet	242.93 m/s
Exhaust Inlet	416.38 m/s
Exhaust Outlet	327.55 m/s

Laminar Model Velocity Magnitudes	
Air Inlet	114.54 m/s
Air Outlet	222.12 m/s
Exhaust Inlet	403.73 m/s
Exhaust Outlet	322.74 m/s

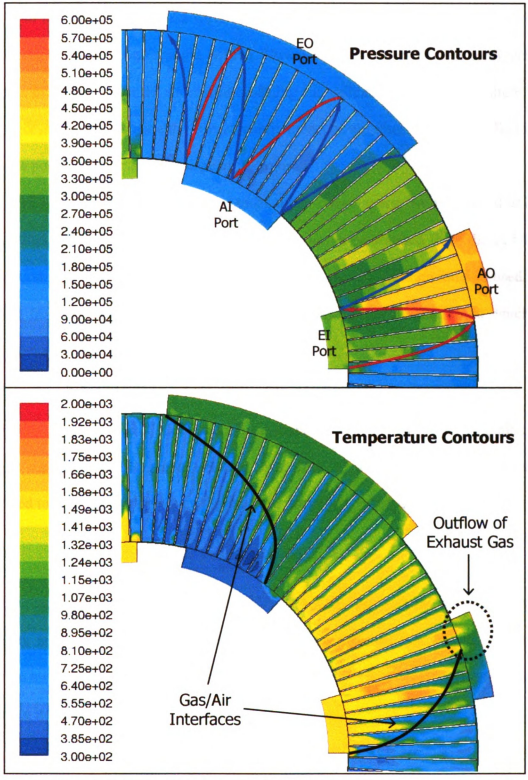

Figure 39. Pressure and temperature contours for final wave pattern iteration using a laminar solver

6.3 ENERGY CONSIDERATIONS

In the previous section, a wave disc design is developed and validated for a rotor with straight channels and straight porting. However, this is an inefficient configuration in terms of energy. After the successful modeling and validation of the wave pattern, it is then necessary to investigate the energy requirements of the rotor. These are affected by both the porting angles and the shape of the rotor.

In order to rotate, the wave disc must either extract energy from the fluid or have is supplied by a motor. This amount of energy may be determined from the FLUENT simulation results. In order to do this, Euler's turbomachinery equation must be used. It is derived from the law of conservation of angular momentum [6]. The rate at which the rotor does work on a fluid is

$$\tau \cdot \omega = \dot{m}\left(U_2 c_{\theta 2} - U_1 c_{\theta 1}\right) \tag{16}$$

where the blade speed is $U = \omega r$, and the subscripts indicate 1 – inlet and 2 – outlet. The c_θ term represents the tangential velocity component of the flow. This equation can be modified to give the work done on the fluid per unit mass, the specific work.

$$\Delta W = \frac{\dot{W}}{\dot{m}} = \omega\left(r_2 c_{\theta 2} - r_1 c_{\theta 1}\right) \tag{17}$$

If the equation results in a positive value, the rotor adds energy to the flow. In this case, the rotor needs to be driven by a motor. If the equation results in a negative value, the rotor extracts energy from the flow. In this case, the rotor would generate torque, allowing it to drive a generator or other device.

Using FLUENT, it is possible to determine the specific work done on or by the fluid. The rotational speed of the rotor is known, and the tangential velocities at the rotor

inlet and outlet can be computed. These are computed as mass-weighted averages on the inner and outer boundaries of the rotating disc.

In the following section, the energy requirements of three separate wave discs will be calculated. First, the final simulation from the previous section will be analyzed. The second design will include angled porting, while maintaining straight channels. The third design will use curved channels in an attempt to extract energy from the flow. The port timing for all three designs will be the final port timing developed in the previous section. The operating conditions will also match.

The first design consists of straight channels and straight ports. The pressure and temperature contours for it were shown in Figure 38. The specific work is calculated using Equation (17) and the values shown in Table 11. The two tangential velocity values were determined by FLUENT. The resulting specific work for this simulation is 57.2 kJ/kg. The value is positive, implying that the disc would have to be driven by an external motor.

Table 11. Values and resulting specific work for final porting design with straight channels and ports

Calculation Values	
r_1	0.005 m
r_2	0.008 m
$c_{\theta 1}$	35.04 m/s
$c_{\theta 2}$	249.72 m/s
ω	31400 rad/s
Result	
ΔW	57.2 kJ/kg

With straight channels and ports, the previous design does not take into account the tangential velocity of the rotor at the inlets and outlets. The straight ports assume that

the flow entering and exiting the channels is completely radial, which is not the case. Since the channel is rotating, the flow also has a large tangential component. The second design in this section uses angled porting to take this into account. In this design, the porting angles are calculated so that the inlet and outlet flows have a tangential velocity component equal to the tangential speed of the channel. The relative velocity angles of the flow at each port are equal to 90°, matching the channel wall shape. The calculated inlet and outlet angles are given in Table 12. With this configuration, the channels do not need to increase the tangential velocity of the flow at the inlets. This should reduce the work required to spin the rotor.

Table 12. Inlet and outlet port angles for a straight channel rotor, shown in Figure 40

Porting Angles	
θ_{EI}	30°
θ_{AI}	54°
θ_{AO}	58°
θ_{EO}	51°

The numerical simulation for this porting configuration uses the same port geometry and operating conditions as the final example in the previous section. The only difference is the slant in the ports. The simulation results are shown in Figure 40. The specific work for this design is calculated using Equation (17) and the values shown in Table 13.

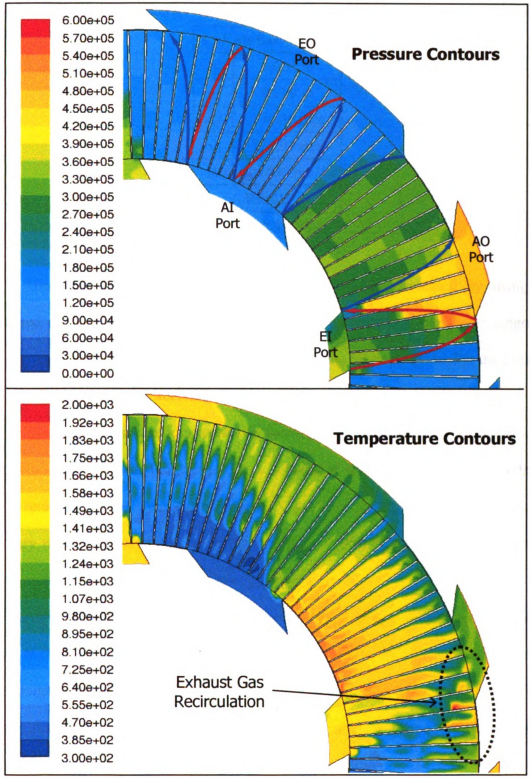

Figure 40. Pressure and temperature contours for a wave disc with angled porting

Table 13. Values and resulting specific work for wave disc with straight channels and angled ports

Calculation Values	
r_1	0.005 m
r_2	0.008 m
$c_{\theta 1}$	134.39 m/s
$c_{\theta 2}$	228.99 m/s
ω	31400 rad/s
Result	
ΔW	36.4 kJ/kg

The work requirement of the rotor is significantly decreased by using the calculated angled porting. Since the inlet air already contains a significant tangential velocity component, the rotor had to do less work on the flow. Additionally, the pressure contours are not altered between this design and the previous with straight porting.

The temperature contours present an increase in the amount of EGR present in the rotor. While the previous design was very successful at scavenging the rotor, this design fails to remove all the exhaust gas before the EO port closes. The port timing and channel geometry remain the same, and so do the boundary conditions at the inlets and outlets. The velocities in the rotor, however, have decreased.

As with traditional turbomachinery, the channels in the wave disc are imparting energy to the flow. This causes an increase to the kinetic energy of the flow. The design with straight porting increased the energy of the fluid more than the design with angled porting. As a result, the fluid velocities within the rotor are higher in the first design. In this configuration with angled porting, the fluid velocities are lower, resulting in larger amounts of EGR.

The final iteration of the wave disc uses curved channels to improve the energy extraction within the rotor. The objective of this design is to be able to extract energy from the flow, while remaining in the same operating point. In order to do this, the curvature of the channel was calculated so that the exhaust outlet would have a tangential velocity component of zero. The curvature developed decreases the tangential velocity of the flow between the inlet and outlet, extracting energy from the flow.

Two important factors have to be taken into account when designing a wave disc with curved channels. The first factor is the increase in channel length. For a disc with equal inlet and outlet diameters, curved channels have a longer arc length than straight channels. This has to be taken into account for the porting design. The first possible solution is to redesign the porting with the increased length. The second, more simple solution is to decrease the outer radius of the rotor until the curved channel has an equal arc length to the original straight channel.

The waves present in the rotor will follow the shape of channels as they travel across them. The resulting wave motion is very different from that of the previous discs. The shockwaves reach the end of the channel in the same amount of time, but due to the curvature, that point is now different than for a straight channel. To correctly design the port timing, the porting on the rotor outlet needs to be offset by an amount equal to the difference in angle between the leading edge and trailing edge of the channel.

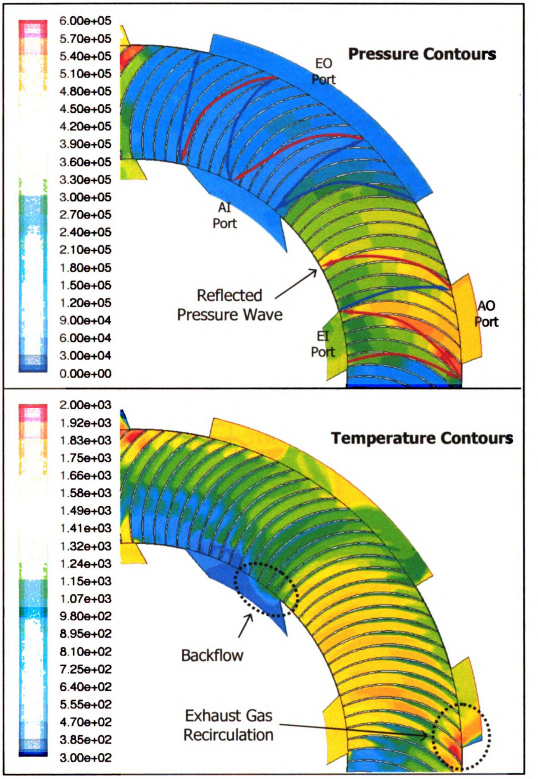

Figure 41. Pressure and temperature contours for a wave disc with curved channels

The final simulation presented includes all of the above conditions. The inlet porting is angled, increasing the tangential velocity at the inlet. The channels are curved to decrease the tangential velocity of the flow to zero at the outlets. It uses a smaller outer radius in order to use the same porting design as the previous simulations. The outlet porting is also offset to allow for the curvature of the channels. The results of the simulation are shown in Figure 41. The values used and the results of the specific work calculation are shown in Table 14.

Table 14. Values and resulting specific work for wave disc with curved channels

Calculation Values	
r_1	0.005 m
r_2	0.00765 m
$c_{\theta 1}$	63.99 m/s
$c_{\theta 2}$	27.10 m/s
ω	31400 rad/s
Result	
ΔW	-3.5 kJ/kg

The work extracted by the rotor is found to be 3.5 kJ/kg. The negative sign in the result indicates that the energy is extracted from the flow. While this is a relatively small amount, the rotor itself is very small compared to traditional turbomachinery. This is enough for the rotor to be self-driving, requiring no external work input.

The pressure contours from this model show the pressure and expansion waves following the channel shape. The wave pattern, however, remains the same. The same set of shockwaves and expansion wave are present, they just follow a more curved path. The temperature contours show the same characteristics present in the previous simulation.

Since the channels no longer add energy to the flow, its velocity is less than that of the previous designs. This results in increased EGR and increased backflow at the AI port.

For micro power generation, the energy extraction for the rotor could be increased even further by improving the channel curvature and the inlet porting angles. The port timing could be improved further to decrease the outflow in the AI port and the amount of EGR. Furthermore, the solution could be optimized to find the maximum power generation for a single design.

As with radial flow turbines, it is much more challenging to extract energy from the flow when it is flowing from the inner radius to the outer radius. The higher blade speeds at the outer radius make it easier to extract energy if the flow enters from there. However, the simulation results prove that even for this flow configuration, the wave disc can extract energy from the flow while still maintaining the correct boundary conditions.

CHAPTER 7: SUGGESTIONS FOR FUTURE WORK

7.1 OPTIMIZATION FOR NUMERICAL SIMULATION CODE

The 2-D numerical code has proven to be a very effective tool toward the creation of successful wave disc designs. The code also has a large potential benefit towards creating an automated optimization process. Currently, the multiple iterations of the numerical code are analyzed and initiated by an engineer. The iterations are repeated until a satisfactory design is complete. It would be even more beneficial if this process could be automated until an optimum solution is achieved.

The 2-D numerical simulation code is set up so that this may be an option for the future. All the code requires is a set of input matrices, and without any other input from the user, it runs through the modeling, meshing, and simulation processes. This flexibility is ideal for optimization software. One such program available is HEEDS. This software may be used to automate the deign methodology presented in the previous chapters. It may even be used to improve the designs further than what can be done manually.

The optimization may be completed with various goals. The software may be used to find the best solution for porting angles, where the most accurate outlet and inlet velocities are obtained. More importantly, though, it may be used to develop the best solution for channel curvature. The software could be programmed in such a way that it will optimize the size and curvature of the channels in order for the rotor to produce the maximum amount of power output possible.

7.2 CFD Simulations of Internal Combustion Wave Disc Engine

Currently there exist three major challenges for micro-scale internal combustion wave disc engines [2, 32]. The first deals with mixing processes. Long mixing times, due to the laminar flow in the channels, result in an uneven mixture of fuel and air. The second challenge is micro-scale combustion and its residence time. The fuel/air mixture must remain in the channel long enough to combust completely. Preliminary experimental and numerical investigations for micro-scale combustion issues have been performed using stationary channels [23,24]. The last issue is with heat transfer and heat loss. The temperature gradients in the device are much larger due to the smaller size of the engine components. The larger gradients result in larger amounts of heat lost to the environment. This decreases the thermal efficiency of the combustion process.

The effect of the described issues on the feasibility of the wave disc engine needs to be studied. Numerical simulation of the IC wave disc engine will be necessary. For this purpose, the 2-D simulation code developed may provide a good starting point. The geometry for the IC wave disc will be very similar to that of a pressure-exchange wave disc, and most of the simulation process as well.

With combustion occurring within the channels themselves, the shape of the channels becomes a major influence to the engine's effectiveness. The multiple different processes occurring within the rotor all have different requirements. The fresh air must enter the rotor and be compressed before combustion. For the combustion process, it is preferable to have an even distribution of fuel and air and a larger channel. After combustion the exhaust gas must be scavenged while extracting energy in the form of usable work.

One of the benefits of the 2-D simulation code developed is that it has no constraints on the channel geometry. It is possible to use it to create a channel with any curvature, even one that is made up of two or three separate curves. The inlet and outlet sides of the channel may be curved, allowing for compression and expansion of the air. The center of the channel may be straight and larger than the inlet and outlet sides, providing a larger width for better combustion. Also, the thinner walls in the combustion zone might improve combustion efficiency by keeping that area hot. The thicker walls in the rest of the channel will help keep wall conduction low in those areas. One such example geometry with its corresponding mesh can be seen in Figure 42.

The channel mesh shown below was developed using the 2-D code presented in Chapter 5. Before the IC wave disc may be modeled some major modifications must be made to the code. The first is the removal of the two extra ports present in the pressure-exchange wave rotor. The second and most challenging change will involve the modeling of the combustion process.

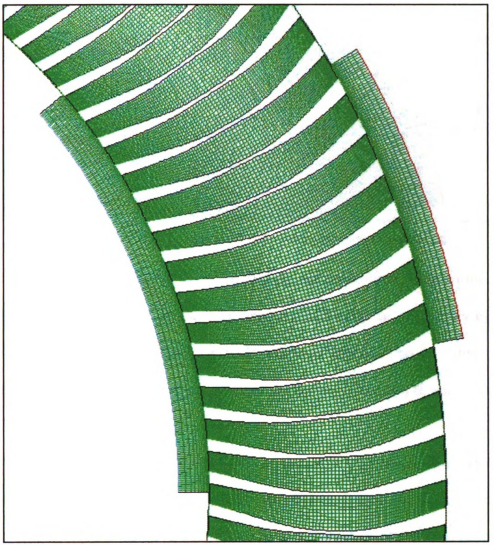

Figure 42. Possible geometry and mesh for the channels of an internal wave disc engine

There are multiple ways to model combustion in FLUENT. The simplest of these to implement would be to simply add heat to the channels at the point where combustion would occur. To create a more accurate model, it would be necessary to take partial combustion and heat losses into account. A simplified method to do this would be to define separate areas within each channel where combustion is expected to occur. The heat addition could then only occur in those areas. Such an example is shown in Figure 43.

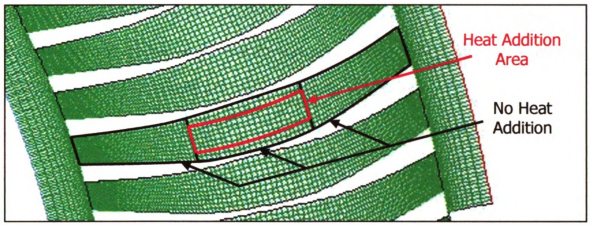

Figure 43. Heat addition zone for internal combustion wave disc modeling

The modeling process for the wave disc engine would have to be unsteady. The channels rotate, and the fluid within them only needs to combust once every cycle. At any point in time, only a few of the channels will have heat addition activated, and the rest will not. As the time step changes, some of the active areas turn off, and some of the deactivated areas must turn the heat addition on.

There is no feedback from FLUENT to the MATLAB code. The code cannot interact with FLUENT; it can only give it commands. As a result, the timing of the heat addition to each channel has to be determined by MATLAB before the simulation is run. In order to control this process correctly, MATLAB must tell the FLUENT simulation which channels will have heat transfer and which will not for each time step. The large number of channels and the large number of time steps for a single simulation will require some major modifications to the simulation code.

Finally, the combustion in the channels could be modeled using FLUENT's species transport and reaction modeling. The air/fuel mixture in the channel may be defined using molar percentages during pre-processing. The channels could then have an intermittent, high temperature igniter modeled within them. This igniter would follow the

same timing as the heat addition process explained above. The FLUENT model will then calculate the heat released by the reaction in a more realistic manner than just simple heat addition, including heat losses and partial combustion of the fuel.

CHAPTER 8: CONCLUSIONS

Two concept engines are presented, the Internal Combustion and External Combustion Wave Disc Engines. This work presents a design methodology for wave discs, which are the main component in these engines. Wave patterns for each engine type have been developed and numerical simulation and validation has been completed for pressure-exchange wave discs.

The automated simulation code developed successfully creates and runs FLUENT simulations for wave discs. The geometry definition and meshing process is flexible enough to adapt to multiple different applications. The time required to complete a single simulation has been reduced significantly. Additionally, the process is completely automatic; it only requires the user to change the input variables to match the desired design.

The 1-D design code has been proven to develop a good initial design for wave disc porting. The improved wave pattern has proven to be more effective at scavenging the rotor than the simple wave pattern. However, it uses many simplifying assumptions, and should only be used as a starting or initial design for numerical simulations.

The iterative design methodology presented is a successful method of studying and developing wave disc designs. It would not be possible to use this methodology without the development of the 1-D design code and the automated numerical simulation code.

Finally, the wave disc energy requirements have been simulated for a set of discs. It has been proven that using angled porting with straight channels, the amount of energy required to drive the rotor may be reduced. Additionally, using curved channels would

allow the rotor extract energy from the flow. The wave disc may be successfully designed to be self-driven or to generate energy.

Using the correct combination of angled porting and channel curvature, it would be feasible for the wave disc to extract enough energy to run a generator. The wave disc operating point is not modified, though. It provides the same compression to the inlet air and the same expansion of the exhaust gas. This proves that the Wave Disc Engine concepts presented are feasible, using the wave disc as a compression-expansion and power generation device.

APPENDIX

Table 15. Geometric and operating conditions for wave disc simulation of simple wave pattern. Results shown in Figure 36.

r_{inner}	5 mm
gap_{inner}	0.03 mm
L_{inner}	0.97 mm
r_{outer}	8 mm
gap_{outer}	0.03 mm
L_{outer}	0.97 mm
θ_{EI}	0°
θ_{AI}	0°
θ_{AO}	0°
θ_{EO}	0°

$\theta_{EI\ open}$	0°
$\theta_{EI\ close}$	16°
$\theta_{AI\ open}$	39°
$\theta_{AI\ close}$	58°
$\theta_{AO\ open}$	9°
$\theta_{AO\ close}$	26°
$\theta_{EO\ open}$	28°
$\theta_{EO\ close}$	42°
c	4 cycles/revolution

$N_{channels}$	120 channels	
r/ΔR	θ	φ/ΔΦ
0	0°	0.8889
1	0°	0.8889

grid unit	mm
P_{ref}	101,325 Pa
Ω	350000 rpm = 36650 rad/s
Δt	2.5×10^{-8} s
$\Delta t_{iterations}$	20
N_{cycles}	6

P_{EI}	400,000 Pa
T_{EI}	1589 K
P_{AI}	150,000 Pa
T_{AI}	435 K
P_{AO}	450,000 Pa
T_{AO}	542 K
P_{EO}	162,000 Pa
T_{EO}	1500 K

Table 16. Geometric and operating conditions for wave disc simulation of improved wave pattern. Results shown in Figure 37.

r_{inner}	5 mm
gap_{inner}	0.03 mm
L_{inner}	0.47 mm
r_{outer}	8 mm
gap_{outer}	0.03 mm
L_{outer}	0.47 mm
θ_{EI}	0°
θ_{AI}	0°
θ_{AO}	0°
θ_{EO}	0°

$\theta_{EI\ open}$	0°
$\theta_{EI\ close}$	19°
$\theta_{AI\ open}$	47°
$\theta_{AI\ close}$	76.5°
$\theta_{AO\ open}$	4.5°
$\theta_{AO\ close}$	23.5°
$\theta_{EO\ open}$	39°
$\theta_{EO\ close}$	85°
c	4 cycles/revolution

$N_{channels}$	120 channels	
$r/\Delta R$	θ	$\varphi/\Delta\Phi$
0	0°	0.8889
1	0°	0.8889

grid unit	mm
P_{ref}	101,325 Pa
Ω	300000 rpm = 31420 rad/s
Δt	2.5×10^{-8} s
$\Delta t_{iterations}$	20
N_{cycles}	6

P_{EI}	400,000 Pa
T_{EI}	1589 K
P_{AI}	150,000 Pa
T_{AI}	435 K
P_{AO}	450,000 Pa
T_{AO}	542 K
P_{EO}	162,000 Pa
T_{EO}	1500 K

Table 17. Geometric and operating conditions for wave disc simulation of final iteration of wave pattern. Results shown in Figure 38 and Figure 39.

r_{inner}	5 mm
gap_{inner}	0.03 mm
L_{inner}	0.47 mm
r_{outer}	8 mm
gap_{outer}	0.03 mm
L_{outer}	0.47 mm
θ_{EI}	0°
θ_{AI}	0°
θ_{AO}	0°
θ_{EO}	0°

$\theta_{EI\ open}$	0°
$\theta_{EI\ close}$	16°
$\theta_{AI\ open}$	47°
$\theta_{AI\ close}$	76.5°
$\theta_{AO\ open}$	9°
$\theta_{AO\ close}$	23°
$\theta_{EO\ open}$	39°
$\theta_{EO\ close}$	85°
c	4 cycles/revolution

$N_{channels}$	120 channels	
$r/\Delta R$	θ	$\varphi/\Delta\Phi$
0	0°	0.8889
1	0°	0.8889

grid unit	mm
P_{ref}	101,325 Pa
Ω	300000 rpm = 31420 rad/s
Δt	2.5×10^{-8} s
$\Delta t_{iterations}$	20
N_{cycles}	6

P_{EI}	400,000 Pa
T_{EI}	1589 K
P_{AI}	150,000 Pa
T_{AI}	435 K
P_{AO}	450,000 Pa
T_{AO}	542 K
P_{EO}	162,000 Pa
T_{EO}	1500 K

Table 18. Geometric and operating conditions for wave disc simulation with angled porting. Results shown in Figure 40.

r_{inner}	5 mm
gap_{inner}	0.03 mm
L_{inner}	0.47 mm
r_{outer}	8 mm
gap_{outer}	0.03 mm
L_{outer}	0.47 mm
θ_{EI}	30°
θ_{AI}	54°
θ_{AO}	58°
θ_{EO}	51°

$\theta_{EI\ open}$	0°
$\theta_{EI\ close}$	16°
$\theta_{AI\ open}$	47°
$\theta_{AI\ close}$	76.5°
$\theta_{AO\ open}$	9°
$\theta_{AO\ close}$	23°
$\theta_{EO\ open}$	39°
$\theta_{EO\ close}$	85°
c	4 cycles/revolution

$N_{channels}$	120 channels	
$r/\Delta R$	θ	$\varphi/\Delta\Phi$
0	0°	0.8889
1	0°	0.8889

grid unit	mm
P_{ref}	101,325 Pa
Ω	300000 rpm = 31420 rad/s
Δt	2.5×10^{-8} s
$\Delta t_{iterations}$	20
N_{cycles}	6

P_{EI}	400,000 Pa
T_{EI}	1589 K
P_{AI}	150,000 Pa
T_{AI}	435 K
P_{AO}	450,000 Pa
T_{AO}	542 K
P_{EO}	162,000 Pa
T_{EO}	1500 K

Table 19. Geometric and operating conditions for wave disc simulation with curved channels. Results shown in Figure 41.

r_{inner}	5 mm
gap_{inner}	0.03 mm
L_{inner}	0.47 mm
r_{outer}	7.65 mm
gap_{outer}	0.03 mm
L_{outer}	0.47 mm
θ_{EI}	30°
θ_{AI}	57.3°
θ_{AO}	19.7°
θ_{EO}	0°

$\theta_{EI\ open}$	0°
$\theta_{EI\ close}$	16°
$\theta_{AI\ open}$	47°
$\theta_{AI\ close}$	76.5°
$\theta_{AO\ open}$	1°
$\theta_{AO\ close}$	15°
$\theta_{EO\ open}$	31°
$\theta_{EO\ close}$	77°
c	4 cycles/revolution

$N_{channels}$	120 channels	
r/ΔR	θ	φ/ΔΦ
0	0°	0.8889
0.1	0.4120°	0.8889
0.2	0.4789°	0.8889
0.3	0.2506°	0.8889
0.4	-0.2414°	0.8889
0.5	-0.9795°	0.8889
0.6	-1.9579°	0.8889
0.7	-3.1836°	0.8889
0.8	-4.6790°	0.8889
0.9	-6.4908°	0.8889
1.0	-8.7112°	0.8889

grid unit	mm
P_{ref}	101,325 Pa
Ω	300000 rpm = 31420 rad/s
Δt	2.5×10^{-8} s
$\Delta t_{iterations}$	20
N_{cycles}	6

P_{EI}	400,000 Pa
T_{EI}	1589 K
P_{AI}	150,000 Pa
T_{AI}	435 K
P_{AO}	450,000 Pa
T_{AO}	542 K
P_{EO}	162,000 Pa
T_{EO}	1500 K

REFERENCES

[1] Aichlmayr, H. T., Kittelson, D. B. and Zachariah, M. R., *"Micro-HCCI Combustion: Experimental Characterization and Development of a Detailed Chemical Kinetic Model with Coupled Piston Motion."* Combustion and Flame, Vol. 135, No. 3, 2003, pp. 227-248

[2] Akbari P., Nalim, M. R., Müller, N., *"Wave Disc Engine for Micro-Scale Power Generation."* AIAA/ASME/SEA/ASEE Joint Propulsion Conference and Exhibit, 2008

[3] Anderson, J. D., *"Modern Compressible Flow: with Historical Perspective."* McGraw-Hill, Third Edition, New York, 2003

[4] Courant, R., Friedrichs, K. and Lewy, H., *"On the Partial Difference Equations of Mathematical Physics."* IBM Journal of Research and Development, Vol. 11, March 1967, pp. 215-234

[5] Dhuler, V.R., et al., *"A Comparative Study of Bearing Designs and Operational Environments for Harmonic Side-Drive Micromotors."* Proceedings IEEE Workshop on Micro Electro Mechanical Systems, February 1992, pp.171-176

[6] Dixon, S. L., *"Fluid Mechanics and Thermodynamics of Turbomachinery."* Elsevier Butterworth-Heinemann, Fifth Edition, Burlington MA, 2005

[7] Epstein, A. H., "*Millimeter-scale, MEMS gas turbine engines.*" Proceedings American SME Turbo Expo 2003 GT-2003-38866, Atlanta, June 2003, pp. 16–19

[8] Epstein, A. H., et al., *"Micro-Heat Engines, Gas Turbines, and Rocket Engines - The MIT Microengine Project."* 28th AIAA Fluid Dynamics Conference, 1997

[9] Epstein, A. H., et al., *"Shirtbutton-Sized Gas Turbines: The Engineering Challenges of Micro High Speed Rotating Machinery."* Proceedings of 8th International Symposium on Transport Phenomena and Dynamics of Rotating Machinery, Honolulu, January 2000

[10] Fernandez-Pello, A. C., *"Micropower Generation Using Combustion: Issues and Approaches."* Proceedings of the Combustion Institute, Vol. 29, 2002 pp. 883-889

[11] Fernandez-Pello, A. C., et al., *"Design and Fabrication of a Silicon-Based MEMS Rotary Engine."* Proceedings International Mechanical Engineering Congress and Exposition, New York, November 2001

[12] Flynn, P. F., et al., *"Meeting the Energy Needs of Future Warriors."* Committee on Soldier Power/Energy Systems, National Research Council, 2004

[13] Grasmeyer, J. M. and Keennon, M.T., *"Development of the Black Widow Micro Air Vehicle."*, American Institute of Aeronautics and Astronautics, 2001

[14] Holladay, J. D., et al., *"Miniature Fuel Processors for Portable Fuel Cell Power Supplies."* Materials Research Society Symposium, 2003

[15] Iancu, F. and Müller, N., *"Efficiency of Shock Wave Compression in a Microchannel."* Journal of Microfluidics and Nanofluidics, 2005

[16] Iancu, F., *"Integration of a Wave Rotor to an Ultra-Micro Gas Turbine (UμGT)."* Doctoral Dissertation, Department of Mechanical Engineering, Michigan State University, 2005

[17] Iancu, F., Akbari, P., and Müller, N., *"Feasibility Study of Integrating Four-Port Wave Rotors into Ultra-Micro Gas Turbines (UμGT)."* 40th AIAA/ASME/SEA/ASEE Joint Propulsion Conference and Exhibit, Florida, 2004

[18] Iancu, F., Piechna, J. and Müller, N., *"Numerical Solutions for Ultra-Micro Wave Rotors."* International Mechanical Engineering Conference, November 2004

[19] Jacobson, S. A. and Epstein, A.H., *"An Informal Survey of Power MEMS."* International Symposium on Micro-Mechanical Engineering, 2003

[20] Koeneman, P. B., Busch-Vishniac I. J. and Wood, K. L., *"Feasibility of Micro Power Supplies for MEMS."* Journal of Microelectromechanical Systems, Vol. 6 No. 4, 1997

[21] Mayer, A., et al., *"Extruded Ceramic – A New Technology for the Comprex® Rotor."* SAE Paper 890453, 1989

[22] Müeller, N., et al., *"An Electric Flight Concept."* 3rd International Symposium on Innovative Aerial/Space Flyer Systems, Tokyo, 2006, pp. 73-80

[23] Nalim, M. R. and Paxson, D.E., *"A Numerical Investigation of Premixed Combustion in Wave Rotors."* Journal of Engineering for Gas Turbines and Power, Vol. 119, No. 3, 1997, pp.668-675

[24] Nalim, R. and Pekkan, K., *"Internal Combustion Wave Rotors for Gas Turbine Engine Enhancement."* Proceedings of the International Gas Turbine Congress, Tokyo, 200

[25] Peirs, J., Reynaerts, D. and Verplaetsen, F., *"A Microturbine for Electric Power Generation."* Sensors and Actuators, Vol. 113, 2004, pp.86-93

[26] Piechna, J. R., *"Feasibility Study of the Wave Disc Micro-Engine Operation."* Journal of Micromechanics and Microengineering, Vol. 16, 2006, pp.S270-S281

[27] Piechna, J., et al., *"Radial-Flow Wave Rotor Concepts, Unconventional Designs and Applications."* International Mechanical Engineering Conference, ASME, November 2004

[28] Pohořelský, L., Sané P. A., et al., *"Wave Rotor Design Procedure for Gas Turbine Engine Enhancement."* Proceedings of ASME Turbo Expo 2008, Berlin, June 2008

[29] Sané P. A., *"Wave Rotor Test Rig Design Procedure for Gas Turbine Enhancement."* Masters Thesis, Department of Mechanical Engineering, Michigan State University, 2008

[30] Seiko Epson Corp, *"Epson Announces Advanced Model of the World's Largest Micro-Flying Robot."* Press Release, 2004 [Available online at: http://www.epson.co.jp/e/newsroom/news_2004_08_18.htm]

[31] Senesky, M. K., *"Electromagnetic Generators for Portable Power Applications."* Doctoral Dissertation, Department of Electrical Engineering and Computer Sciences, University of California, Berkeley, 2005

[32] Sharma K., *"Preliminary Design Approach to the First Generation Internal Combustion Wave Disc Engine."* Masters Thesis, Department of Mechanical Engineering, Michigan State University, 2008

[33] Turns, S. R., *"An Introduction to Combustion."* McGraw-Hill, Second Edition, New York, 2000

[34] Welch, G. E., *"Wave Engine Topping Cycle Assessment."* American Institute of Aeronautics and Astronautics, 1997

[35] Welch, G. E., et al., *"Wave Rotor-Enhanced Gas Turbine Engine Demonstrator."* Gas Turbine Operation and Technology for Land, Sea and Air Propulsion and Power Systems Symposium, Ottawa, October 1999

[36] Welch, G. E., Jones, S. M., et al., *"Wave Rotor-Enhanced Gas Turbine Engines."* Journal of Engineering for Gas Turbines and Power, Vol. 119, No. 2, 1997, pp. 470-477

[37] Woods, M. I., Henderson, J.F. and Lock, G. D., *"Energy Requirements for the Flight of Micro Air Vehicles."* The Aeronautical Journal, Vol. 105, March 2001, pp.135-147

[38] Yang, W. M., et al., *"Power Generation at the Micro Scale."* International Journal of Computational Engineering Science, Vol. 4, No. 3, 2003, pp.481-484